Cluster radioactivity: progress and perspectives; experiment and theory

Yu. S. Zamyatnin, V. L. Mikheev, S. P. Tret'yakova, and V. I. Furman

Joint Institute for Nuclear Research, Dubna

S. G. Kadmenskiĭ

Voronezh State University, Voronezh

Yu. M. Chuvil'skiĭ

Institute of Nuclear Physics, Moscow State University, Moscow

Fiz. Elem. Chastits At. Yadra **21**, 537–594 (March–April 1990)

Experimental data on the radioactive decay of heavy nuclei with emission of ^{14}C, ^{24}Ne, ^{28}Mg, and ^{32}Si ions obtained up to now are reviewed. The phenomenological systematization of these data is discussed. A review is given of the theoretical approaches to the analysis of this type of nuclear decay, including both models of superasymmetric fission and microscopic calculations. The mechanism of cluster decay is considered, and possibilities for future studies are discussed.

INTRODUCTION

In 1984 two groups working independently in England (Oxford University) (Ref. 1) and in the USSR (I. V. Kurchatov Institute of Atomic Energy) (Ref. 2) discovered the radioactive decay of ^{223}Ra with emission of the ^{14}C nucleus.

By now, radioactive decays with emission of particles of mass intermediate between those of α particles and binary-fission fragments (^{14}C, ^{24}Ne, ^{28}Mg, ^{32}Si) have been discovered for 11 nuclides from radium to plutonium. Over 100 experimental and theoretical publications have already been devoted to the study of this new type of radioactivity.

The first attempt to discover radioactive decay with emission of particles different from helium nuclei was the experiment of Rutherford and Robinson carried out in 1914 (Ref. 3). The question to be answered was very clear: are any charged atoms besides helium atoms and recoil atoms emitted by radioactive matter? In that experiment it was established that if such particles are emitted, the number of them is no more than 10^{-4} of the number of helium atoms.

The existence of radioactivity with emission of fragments of mass intermediate between those of α particles and fission fragments has often been discussed, primarily in connection with certain anomalies in the light-element isotope content in minerals containing uranium. [4,5]

The possible existence, in principle, of any type of decay is primarily determined by its exothermic nature, $Q > 0$. For elements in the second half of the periodic table, whose mean binding energy per nucleon in the nucleus is smaller than for the lighter elements, this requirement is satisfied for a very large number of different types of nuclear decay. However, the overwhelming majority of possible decays are not realized, owing to the extremely small potential-barrier penetration factor. This factor becomes sizable only in two cases: in α decay and in spontaneous fission of heavy nuclei into fragments of roughly equal mass. We note that the barrier penetration factors themselves for the emission of some heavy clusters X, such as ^{14}C, ^{24}Ne, and so on, from the parent nucleus with the formation of a residual nucleus close to the doubly magic nucleus ^{208}Pb can significantly exceed the corresponding values of the penetration factors for α decay. This is related to the fact that the ratios Q_X/B_X are significantly larger than the ratios Q_α/B_α, where $B_{X(\alpha)}$ are the heights of the corresponding barriers. Apparently, aside from the considerable technical difficulties, the main reason for the lack of enthusiasm among investigators was the realization of the fact that the possibility for the formation of a heavy cluster at the surface of a nucleus undergoing decay must be significantly smaller than for an α particle, which can more than compensate the effect of relatively large values of Q_X.

The approach from the viewpoint of fission also did not suggest any reason for optimism. It was well known that the relative yield of fragments falls off sharply as the asymmetry of the fission grows, with the dominant contribution coming from fragments with above-barrier energies of the relative motion, while there is a summation over the large number of fragment excited states in the detection process. The observation of fission products in fixed final states is a very difficult problem. An example is cold fission, the relative yield of which is no larger than 10^{-6}. In the case of emission of the fragments of interest to us, the situation is that of observing cold fission with relative fragment energy much smaller than the corresponding Coulomb barrier.

Nevertheless, persistent enthusiasts in the USSR (the Institute of Atomic Energy) and in England improved the experimental techniques and finally achieved success in 1984. The English were luckiest.[1] They beat their colleagues from the USSR[2] by several months. It should be noted that long before the experimental discovery, back in 1980, theoreticians attempted to draw the attention[6] of the physics community to the possibility and prospects for studying this new type of radioactivity. The authors of Ref. 6 made a fundamental study of two possible cluster emission mechanisms—superasymmetric fission and α decay. However, no quantitative predictions were made in that study. Simply on the basis of maximizing the ratio of the energy yield to the height of the Coulomb barrier, the two groups of experimentalists independently chose to work with the parent nucleus ^{223}Ra. (See Ref. 7 for a first-hand account of the history of this problem.)

In the first part of this review we study the experimental technique and discuss the results of the actual experiments.

 0090-4759/90/020231-26$04.00

We give a preliminary systematics of the cluster half-decay periods. Then we analyze the various theoretical approaches to the description of this new type of radioactivity in detail. These approaches include various models of superasymmetric fission, simple models of the Gamow type, and also microscopic models related to α decay, which explicitly take into account the shell structure of the emitted cluster and of the parent and daughter nuclei. The experimental data are compared with the theoretical calculations for the purpose of determining the mechanism for this decay. In conclusion, we discuss the possibilities and outlook for the study of this new type of radioactivity.

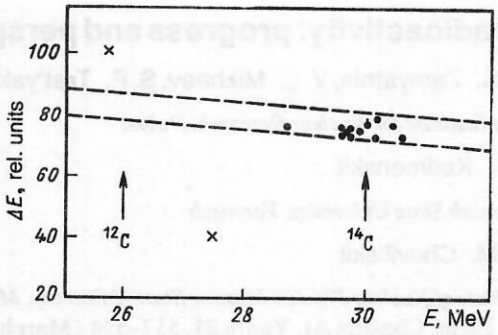

FIG 1. Two-dimensional distribution of ^{223}Ra decays with ^{14}C emission in Ref. 1 for a measurement time of 189 days. The band isolated by the dashed line corresponds to carbon ions. The arrows indicate the ion energies in decay into ^{12}C and ^{14}C: black circles—carbon ions; ×—superposition of four α particles.

1. THE EXPERIMENTAL DISCOVERY OF CLUSTER RADIOACTIVITY

As we mentioned above, the first experimental confirmation of the existence of cluster radioactive decay was the observation of ^{223}Ra decay with ^{14}C emission, made simultaneously by two groups of investigators.[1,2] Each of these groups found about ten events of ^{223}Ra decay in which a ^{14}C nucleus of energy of about 30 MeV was emitted and the resulting daughter nucleus was close to the doubly magic nucleus ^{209}Pb:

$$^{223}\mathrm{Ra} \rightarrow {}^{14}\mathrm{C} + {}^{209}\mathrm{Pb} + Q, \text{where} Q = 31{,}85 \text{ MeV}. \qquad \text{(A)}$$

These experiments showed that the ^{14}C emission probability is almost ten orders of magnitude smaller than the α-decay probability. Naturally, the detection of such rare events on the background of the huge number of α particles was a very complicated technical problem. Therefore, in these experiments the discrimination of carbon nuclei from multiple α-particle pile-up was improved by the simultaneous measurement of two parameters of the decay product using a ΔE–E telescope of semiconductor detectors. This allowed the selection of particles according to both their charge and their energy, which, in turn, gave information about the mass of the emitted particle. Nevertheless, even when this technique was used and the resolution time of the detection system was fairly high ($\tau \sim 50$–100 nsec), the high rate at which α particles hit the detectors imposed an important constraint on the activity of the samples which were used.

A convenient source of radiation was the long-lived isotope ^{227}Ac ($T_{1/2} = 21.7$ yr) existing in equilibrium with its daughter product ^{223}Ra ($T_{1/2} = 11.4$ days). In Ref. 1 the activity of the source was altogether 3.3 μCi, so that a very long time was required to carry out the experiment (194 days for the first series and 189 days for the second).

Owing to the better resolution time of the apparatus and the smaller solid angle used to detect the decay products, in Ref. 2 the measurements could be carried out with a source of higher activity. This made it possible to obtain a comparable effect after 30 days of measurements (Table I).

The measures taken by the authors of these two studies allowed them to fairly reliably select and identify ^{14}C nuclei (Fig. 1). The relative probabilities for ^{14}C emission obtained in these studies coincide within the measurement errors and are $\lambda_C/\lambda_\alpha = (8.5 \pm 2.5) \times 10^{-10}$ in Ref. 1 and $\lambda_C/\lambda_\alpha = (7.6 \pm 3.0) \times 10^{-10}$ in Ref. 2.

An important technical advance was the use of a magnetic field to improve the α-particle discrimination. The first such experiment was carried out at Orsay in 1984 (Ref. 8) using a magnetic spectrometer of large luminosity (a solid angle of ~ 0.1 sr) which eliminated the direct incidence of α particles on the ΔE–E detector located in the focal plane of the spectrometer (Fig. 2). This made it possible to use a more intense ^{223}Ra source (an intensity about 70 times higher than that at Oxford) and significantly shortened the measurement time: 11 events of ^{223} Ra decay were detected during 5 days (Fig. 3).

By means of control and calibration measurements it was determined that emission of the ^{14}C nucleus with energy $E_C = (29.4 \pm 1.2)$ MeV, which is very close to the value 29.8 MeV following from the decay energy, is observed. Beams of accelerated $^{12}C^{6+}$, $^{14}C^{6+}$, and $^{16}O^{8+}$ ions of the corresponding energy were used to calibrate the spectrometer. The relative decay probability λ_C/λ_α was found to be $(5.5 \pm 2.0) \times 10^{-10}$.

A similar experiment with magnetic separation of the

TABLE I. Typical parameters and results of experiments on ^{223}Ra decay.

Activity of the ^{223}Ra target, μCi	Solid angle, sr	Measurement time, days	Number of detected decays	Reference
0,003	1/3	194	8	[1]
		189	11	[1]
0,08	0,1	30	7	[2]
0,21	0,115	5	11	[8]
9,2	$5 \cdot 5 \cdot 10^{-3}$	6	24	[9]

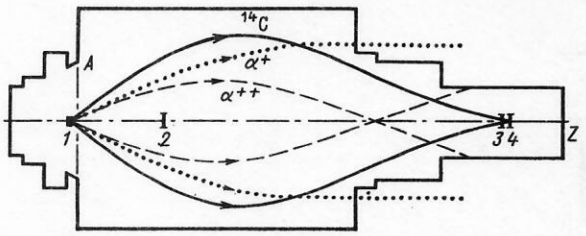

FIG. 2. Schematic depiction of the setup for ^{14}C detection with magnetic separation of α particles from carbon ions in Ref. 8: 1—source; 2—shield from the direct beam; 3, 4—(ΔE–E) telescope.

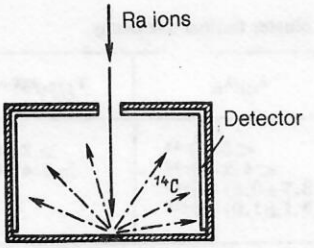

FIG. 4. Geometry of the experiment of Price *et al.* at CERN (Ref. 10).

decay products was carried out later (in 1985) at Argonne National Laboratory by Kutschera *et al.*[9] An even more intense ^{223}Ra source was used in this experiment, and ^{227}Th ($T_{1/2} = 18.7$ days) was used as the parent matter. The mean ^{223}Ra activity during the experiment was 9.2 mCi.

Since the magnetic spectrograph used to separate the α particles had a significantly lower luminosity ($\sim 5\times10^{-3}$ sr), the rate of detection of carbon nuclei was increased altogether by a factor of 2. However, use of the spectrograph made it possible to directly determine the mass of the emitted particles and measure their energy more accurately. This

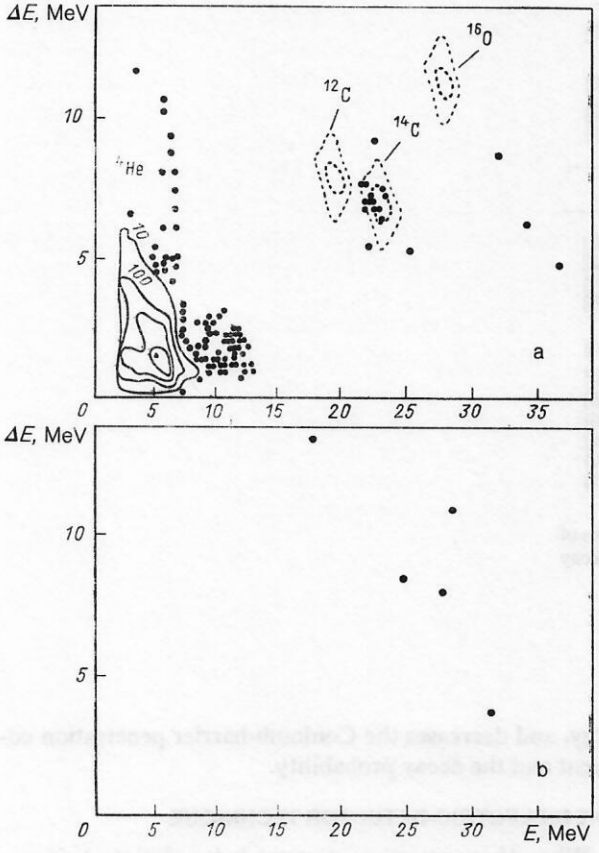

FIG. 3. Distribution of ^{223}Ra decays in Ref. 8: a—detection of ^{223}Ra decays; b—background events (without the source).

increased the certainty that the ^{14}C nucleus is emitted in ^{223}Ra decay, and the expected decay energy was confirmed to within $\pm$ 0.2 MeV.

The spectrograph was calibrated using ^{14}C ions accelerated by an electrostatic tandem generator operating in the regime of measuring very small concentrations of long-lived radioisotopes.

An original experimental setup different from those of preceding studies was used in the work of Price *et al.*[10] In this experiment ^{221}Fr, ^{221}Ra, ^{222}Ra, ^{223}Ra, and ^{224}Ra isotopes were obtained from the splitting of thorium by protons of energy 600 MeV at the CERN synchrocyclotron, and were then separated on-line by the ISOLDE mass separator and implanted inside cylinders whose walls were covered on the inside with a polycarbonate film serving as a detector of the decay products (Fig. 4).

After processing by track detectors (see below), the decay under study was discovered to occur not only in ^{223}Ra, but also in two isotopes of radium, ^{222}Ra and ^{224}Ra. Its relative probability for these isotopes proved to be even smaller: $(3.7 \pm 0.6)\times10^{-10}$ for ^{222}Ra and $(4.3 \pm 1.2)\times10^{-11}$ for ^{224}Ra. The effect was not discovered for the isotopes ^{221}Fr and ^{221}Ra. Only its upper limit was determined.

Somewhat later[11] at Orsay, the technique developed there and described above was used to confirm the decay of ^{222}Ra with ^{14}C emission, and a similar form of the decay was found for the fourth radium isotope ^{226}Ra. In Ref. 32 the result for ^{226}Ra decay was confirmed, and lower limits on the ratios λ_C/λ_α for ^{14}C emission from ^{221}Fr, ^{221}Ra, and ^{225}Ac nuclei were determined.

All the results on the observation of the radioactivity of radium isotopes accompanied by emission of the ^{14}C nucleus are summarized in Table II. We see that all the experiments give results in good agreement with each other and quite convincingly show that at least four isotopes of radium undergo this new type of decay.

After the first results on this decay were obtained, the question arose of seeking other types of decay accompanied by emission of ions heavier than ^{14}C, and understanding how the decay probability varies as the number of nucleons in the emitted nucleus increases. Experiments on this were begun in 1984 at Dubna[12] and at Berkeley.[13] The group at Berkeley decided to use the nuclide ^{232}U, while that at Dubna used ^{231}Pa and light isotopes of thorium and uranium: ^{230}Th and ^{233}U.

These choices originated in the assumption that in all cases of the decay the daughter products must be nuclei close

TABLE II. Experimental results on cluster radioactive decay.

Initial nucleus	Emitted cluster	Decay energy Q, MeV	$\lambda_{Cl}/\lambda_\alpha$	$T_{1/2}$, yr	Reference
^{221}Fr	^{14}C	31,28	$<5\cdot10^{-14}$	$>2\cdot10^{8}$	[32]
^{221}Ra	^{14}C	32,39	$<1,2\cdot10^{-13}$	$>7\cdot4\cdot10^{6}$	[32]
^{222}Ra	^{14}C	33,05	$(3,7\pm0.6)\cdot10^{-10}$		[10]
			$(3.1\pm1.0)\cdot10^{-10}$		[11]
Weighted mean value			$(3.5\pm0.5)\cdot10^{-10}$	$(3,4\pm0.5)\cdot10^{3}$	
^{223}Ra	^{14}C	31,85	$(8.5\pm2.5)\cdot10^{-10}$		[1]
			$(7.6\pm3.0)\cdot10^{-10}$		[2]
			$(5.5\pm2.0)\cdot10^{-10}$		[8]
			$(4.7\pm1.3)\cdot10^{-10}$		[9]
			$(6.1\pm1.0)\cdot10^{-10}$		[10]
Weighted mean value			$(5.9\pm0.7)\cdot10^{-10}$	$(5,3\pm0.6)\cdot10^{7}$	
^{224}Ra	^{14}C	30,54	$(4,3\pm1,2)\cdot10^{-11}$	$(2.3\pm0,6)\cdot10^{8}$	[10]
^{226}Ra	^{14}C	28,21	$(3,2\pm1,6)\cdot10^{-11}$		[11]
			$(2.9\pm1.0)\cdot10^{-11}$		[32]
Weighted mean value			$(3,0\pm0.8)\cdot10^{-11}$	$(5,3\pm1,4)\cdot10^{13}$	
^{225}Ac	^{14}C	30,47	$<4\cdot10^{-13}$	$>7\cdot10^{10}$	[32]
^{231}Pa	^{23}F	51,84	$<4\cdot10^{-14}$	$>8\cdot10^{17}$	[15]
^{230}Th	^{24}Ne	57,78	$(5.6\pm1.0)\cdot10^{-13}$	$(1.3\pm0,3)\cdot10^{17}$	[26]
^{232}Th	^{26}Ne	55,97	$<5\cdot10^{-11}$	$>3\cdot10^{20}$	[17]
^{231}Pa	^{24}Ne	60,42	$(3.8\pm0,7)\cdot10^{-12}$	$(8.6\pm1.6)\cdot10^{15}$	[15]
^{232}U	^{24}Ne	62,31	$(2.0\pm0,5)\cdot10^{-12}$	$(3.4\pm0.8)\cdot10^{13}$	[13]
^{233}U	^{24}Ne	60,50	$(7,5\pm2,5)\cdot10^{-13}$		[16]
	^{25}Ne	60,85	$(5,3\pm2,3)\cdot10^{-13}$		[17]
Weighted mean value			$(6,3\pm1.7)\cdot10^{-13}$	$(2,5\pm0,7)\cdot10^{17}$	
^{234}U	^{24}Ne	58,84	$(4.4\pm0.5)\cdot10^{-13}$		[23]
	^{26}Ne	59,47	$(3,9\pm1,0)\cdot10^{-13}$		[22]
Weighted mean value			$(4,3\pm0,4)\cdot10^{-13}$	$(5,7\pm0,6)\cdot10^{17}$	
^{235}U	^{24}Ne	57,36			
	^{25}Ne	57,83	$<5\cdot10^{-12}$	$>1,4\cdot10^{20}$	[22]
	^{26}Ne	58,11			
^{236}U	^{24}Ne	55,96			
	^{26}Ne	56,75	$<4\cdot10^{-12}$	$>6\cdot10^{18}$	[22]
^{234}U	^{28}Mg	74,13	$(1,4\pm0,2)\cdot10^{-13}$		[23]
			$(2,3\pm0.7)\cdot10^{-13}$		[22]
Weighted mean value			$(1.5\pm0,2)\cdot10^{-13}$	$(1,6\pm0,2)\cdot10^{18}$	
^{235}U	^{28}Mg	72,20	$<8\cdot10^{-13}$	$>9\cdot10^{20}$	[22]
^{236}U	^{30}Mg	72,51	$<4\cdot10^{-12}$	$>6\cdot10^{18}$	[22]
^{237}Np	^{30}Mg	75,02	$<4\cdot10^{-14}$	$>5\cdot10^{19}$	[26]
^{236}Pu	^{28}Mg	79,67	$\sim 2\cdot10^{-14}$	$\sim 1,5\cdot10^{14}$	[28]
^{238}Pu	^{28}Mg	75,93			
	^{30}Mg	77,03	$(5,6^{+4,4}_{-2,5})\cdot10^{-17}$	$\sim 1,5\cdot10^{18}$	[23]
	^{32}Si	91,21	$(1.4^{+0,6}_{-0,4})\cdot10^{-16}$	$\sim 6.5\cdot10^{17}$	[23]
^{240}Pu	^{34}Si	90,95	$<1,3\cdot10^{-13}$	$>5\cdot10^{16}$	[25]
^{241}Am	^{34}Si	93,84	$<5\cdot10^{-15}$	$>9\cdot10^{16}$	[26]
			$<3\cdot10^{-12}$	$>1.4\cdot10^{14}$	[11]
			$<4.2\cdot10^{-13}$	$>1.0\cdot10^{15}$	[30]
			$<7.4\cdot10^{-16}$	$>5.8\cdot10^{17}$	[31]

Note. For isotopes for which there are several independent experimental determinations of $\lambda_{Cl}/\lambda_\alpha$ we also give their mean weighted values. In these cases we give the half-decay periods $T_{1/2}$ corresponding only to the mean values.

to the doubly magic nucleus ^{208}Pb, so that nuclei heavier than carbon—oxygen, fluorine, and neon—will be emitted in the decay. Lighter isotopes of each element were chosen because, as is well known, the nuclei of heavy elements are weighted down by neutrons. Because of this the decay products also must have a neutron excess, which is larger, the heavier the isotope of the initial element, and which tends to move them far from the stability region, lowers the decay energy, and decreases the Coulomb-barrier penetration coefficient and the decay probability.

2. THE DIELECTRIC-DETECTOR TECHNIQUE

When these experiments were being designed, it was clear that the use of an efficient measurement technique was crucial for their success. From the analysis of experiments with radium isotopes it was seen that the techniques used in

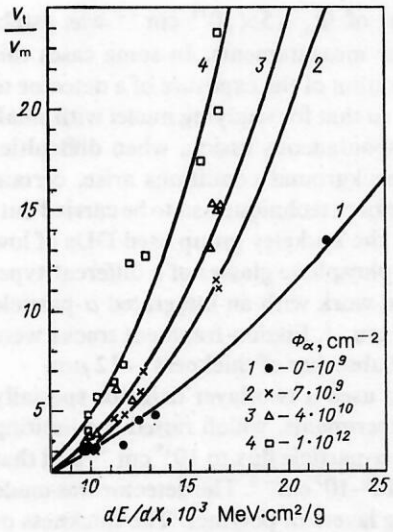

FIG. 5. Dependence of the ratio of the etching rate along a track and the etching rate of plastic v_t/v_m on the specific ionization for various integrated α-particle fluxes. The irradiation was carried out in air in a 2π geometry.

them do not allow the discovery of relatively rare decay modes whose relative probability is less than 10^{-12}. This bound is primarily related to the need to use thin targets of small area in these methods and to the very small fraction (except in the experiments of Price *et al.*) of detected decay products.

It was realized that an effective technique could be based on the use of dielectric detectors (DDs), which are widely used to detect heavy ions and spontaneous nuclear-fission events.

The distinguishing feature of DDs which is crucial for the present problem is the presence of a charged-particle detection threshold determined by the specific ionization of the particle and by the detector material. For example, the polycarbonate used by Price *et al.*[10] detected particles with $Z \geqslant 5$, and the lavsan (polyethylene terephthalate) used at Dubna detected particles with $Z \geqslant 6$, thereby excluding background α particles. In addition, the rate of etching of the detector material along a particle track depends strongly on the specific ionization, which makes it possible to identify the detected particles according to their charge, and leads to a significant difference between the shapes of tracks made by light particles and by fission fragments, which are also registered by the detector.

An important advantage of DDs in the detection of rare events is the possibility of using large amounts of the matter under study in experiments, owing to the large target area (up to 1000 cm^2) and the high efficiency of decay-product detection. All these factors, together with the possibility of long-term exposure of the detector, allow an experimental sensitivity 2–3 orders of magnitude greater than when semiconductor detectors are used.

A characteristic feature of DDs is the need (after their exposure) for chemical etching in the corresponding reagent to increase the cluster tracks to optically visible dimensions. Depending on the identification method which is chosen, one-step etching or multistage successive etching is used. Here the track parameters needed for determining the etching rate of the detector material along a track, v_t, the etching rate of the unexposed material of the DD, v_m, and their ratio, called the etching discrimination, v_t/v_m, are measured after each stage of the etching.

The relation between the etching discrimination v_t/v_m and dE/dX of the ions for a given detector is determined by means of calibration of the detector by accelerated ions with Z from 6 to 18. As an example, in Fig. 5 we show the dependence of v_t/v_m on dE/dX for a polyethylene terephthalate DD for various integrated fluxes of α-particle radiation (see below).

Cluster decay has been studied using DDs by the two groups of investigators—at Berkeley (USA) and at Dubna (USSR)—by different methods.

The American group bombarded the DD in a vacuum. The geometry of the bombardment was chosen so that a cluster entered the DD at an angle to its surface of close to 90°. The configuration of a singly etched track is shown schematically in Fig. 6a for this geometry. In this case clusters were identified using a method in which the track profile was determined using a replica made from a special material. The measured parameters of the replica were transformed into a curve for the dependence $v_t/v_m(R_{res})$, where R_{res} is the residual range of the cluster in question.[33]

In the studies of the Dubna group the bombardment of the DD by radioactive samples was carried out in air in a nearly 2π geometry (Fig. 6b). The etching was done in several successive stages, after each of which the track parameters (diameter of the entrance aperture, projection of the track length on the detector plane) were measured and the values of v_t/v_m and R_{res} were determined, as above. For the cluster identification the DDs were calibrated using ^{16}O, ^{20}Ne, and ^{26}Mg ions accelerated at the JINR U-300 cyclotron to energies of 1.6–2.5 MeV/amu. In order to take into account the effect of the actual radiation conditions on the

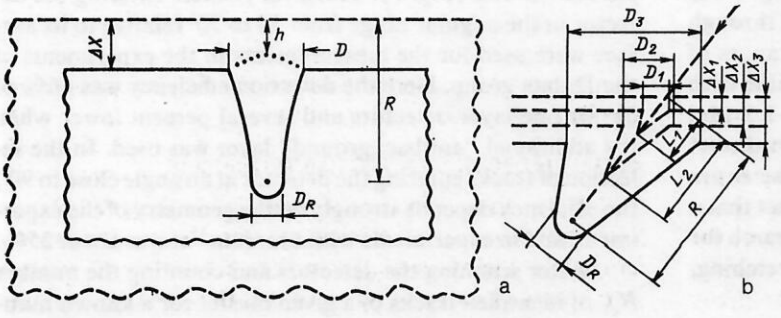

FIG. 6. Schemes for measuring track parameters: (a) Single-stage etching for perpendicular entry of the track into the detector (Ref. 33). ΔX is the thickness of the etching layer of the detector material. Tracks were identified using the relations $v_t/v_m = f(D, \Delta X, h)$, $R_{res} = R - h/2$ and $v_t/v_m = f(D, \Delta X, D_R)$, $R_{res} = R/2$. (b) Multistage (here, three-stage) etching of a track during irradiation in a 2π geometry (Ref. 22). The relations $v_t/v_m = f(D_i, L_i, \Delta X_i)$, $R_{res} = R - L_i/2$ were used to identify a track at several points along its length.

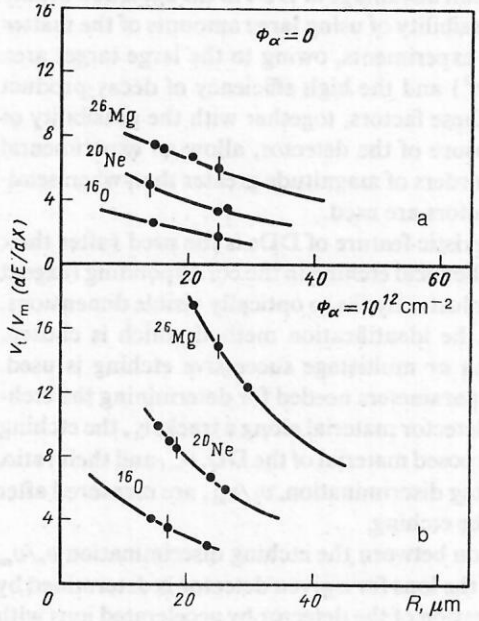

FIG. 7. Calculated dependences of v_t/v_m on the residual range (R_{res}) in a DD for tracks of oxygen, neon, and magnesium ions. The points are the calibration data without additional α-particle irradiation (a), and for an integrated α-particle flux of 10^{12} cm^{-2} (b).

detector sensitivity,[34] calibration experiments were carried out in conjunction with the bombardment of the DD by α particles from the source under study. It can be seen from Fig. 5 that for DDs made of polyethylene terephthalate, the discrimination v_t/v_m grows significantly for an integrated α-particle flux Φ_α above 10^{10} cm^{-2}. The experimental data which were obtained can be expressed by the functional dependence $v_t/v_m = a(dE/dX)^b$, where $a = 0.045$ for $\Phi_\alpha = 0$–10^9 cm^{-2} and $a = 0.0063$ for $\Phi_\alpha > 10^9$ cm^{-2}; $b = 1.83 + 0.81(\Phi_\alpha \times 10^{-9})^{0.04}$. This function can be used to predict the features of the DD as a function of Φ_α. The effect of Φ_α on the identification of cluster tracks is shown in Fig. 7, where we give the dependence $v_t/v_m(R_{res})$. We see that raising the α-particle bombardment improves the cluster identification. This effect is observed only for bombardment in air.

Study of the dependence of the energy dispersion of the calibration ions on Φ_α obtained from the spectral distribution of the ion ranges showed that the dispersion increases markedly for an integrated α-particle flux of $\sim 10^{12}$ cm^{-2}. This is due to the appearance of a large number of etched tracks of oxygen and carbon recoil nuclei appearing in the elastic scattering of α particles which have passed through the detector ($\sim 10^{-6}$ tracks/particle). Since the ranges of the α particles from the samples used are comparable with the ranges of the clusters under study for $E \sim 2$–2.5 MeV/amu, the background tracks of recoil nuclei can distort the shape of a cluster track, intersecting it along the entire range. It is also necessary to take into account the fact that a large number of recoil-nucleus tracks hinders the search for cluster tracks, especially during the first stages of etching, when their length is small, $\sim 10\,\mu$m.

Therefore, a limit of $\Phi_\alpha \sim 5 \times 10^{11}$ cm^{-2} was established for spectrometer measurements. In some cases this limit restricted the duration of the exposure of a detector to the radioactive target, so that for studying nuclei with small α-decay periods and spontaneous fission, when difficulties due to deteriorating background conditions arise, certain changes in the measurement technique had to be carried out.

In relation to this the Berkeley group used DDs of low sensitivity made from phosphate glasses of a different type, which allowed them to work with an integrated α-particle flux of up to 10^{13}–10^{14} cm^{-2}. Fission-fragment tracks were eliminated using an Al absorber of thickness $\sim 12\,\mu$m.

The Dubna group used a two-layer detector specially developed for these experiments, which raised the limiting value of the integrated α-particle flux to 10^{15} cm^{-2} and that of fission fragments to 10^6–10^7 cm^{-2}. The detector was made from two closely fitting layers of polymer. The thickness of the upper layer was chosen in such a way that in the processing regime for which it was designed its residual thickness exceeded the range of recoil nuclei from α-particle elastic scattering by 3–5 μm. Therefore, an etched track of a recoil nucleus, even if it entered the detector perpendicularly, did not reach the lower layer of the detector. After the etching the upper layer was removed.

For studying decays of radium nuclei with carbon cluster emission, the American group used[10,32] DDs made from polycarbonate, which detected carbon ions with $E < 2.5$ MeV/amu. For studying decays of nuclei with $Z \geqslant 90$, the two groups used[13–15] a less sensitive polymer polyethylene terephthalate DD, which detects long-range ions with $Z > 6$ and carbon recoil nuclei of energy ~ 1 MeV/amu, and does not detect α particles.

The DD etching was carried out in a 20% solution of NaOH at a temperature of 60 °C. Visual discrimination in the scanning was carried out either according to the round dark spots of the perpendicular tracks after prolonged etching, or according to cusped tracks in the multistage etching process. The total range of the cluster was measured for complete etching of the track (up to where the particle stops), which is characterized by its rounded tip. The residual range is defined as the difference between the full range and half the length of the cone for each stage of the etching.

The calculated and experimental calibration data were used to construct graphs of the dependence of v_t/v_m on R_{res} for various types of ions, and the experimental points were plotted on them (Fig. 8). The cluster charges were determined, and their mass number was estimated in this manner. The error in the charge identification reached $\Delta Z = \pm 0.15$, and that in the mass identification was $\Delta M = \pm 1$.

The cluster energy was determined from the distribution of the full cluster ranges with a relative error of $\Delta E/E \sim 3$–5% (Fig. 9). Tracks of clusters entering the detector in the angular range from 15 to 70° relative to its surface were used for the measurements in the experiments of the Dubna group. Here the detection efficiency was 66% of 2π for one-layer detectors and several percent lower when the additional "antibackground" layer was used. In the selection of tracks entering the detector at an angle close to 90°, the efficiency depends strongly on the geometry of the experiment, and in experiments with uranium[13] it was about 25%.

After scanning the detectors and counting the number N_{cl} of identified tracks of a given cluster for a known num-

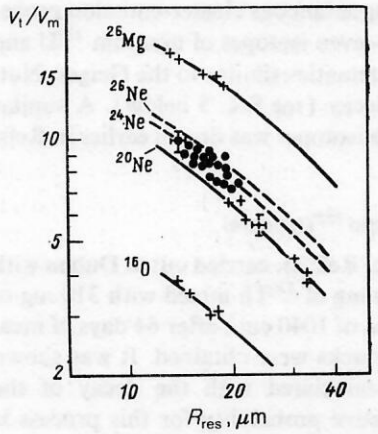

FIG. 8. Dependence of the etching discrimination v_t/v_m on the residual range of the cluster in ^{230}Th decay.

ber of decaying nuclei, the probability for cluster emission relative to that for α decay was found from the expression

$$\lambda_{cl}/\lambda_\alpha = A_{cl}/\epsilon N_\alpha.$$

Here N_α is the calculated number of α particles emitted into the solid angle 2π during the exposure time and ϵ is the cluster detection efficiency for the same solid angle.

3. EMISSION OF Ne, Mg, AND Si CLUSTERS

Experiments with ^{231}Pa and ^{232}U nuclei

The first studies on the observation of spontaneous cluster emission from ^{231}Pa (Ref. 12) and ^{232}U (Ref. 13), carried out at Dubna and Berkeley, were published on the same day, 26 December 1984, in the journals JINR Rapid Communications and Physical Review C, respectively.

In the experiments with the ^{231}Pa isotope carried out at Dubna,[12] a source containing 7 mg (0.35 mCi) of matter

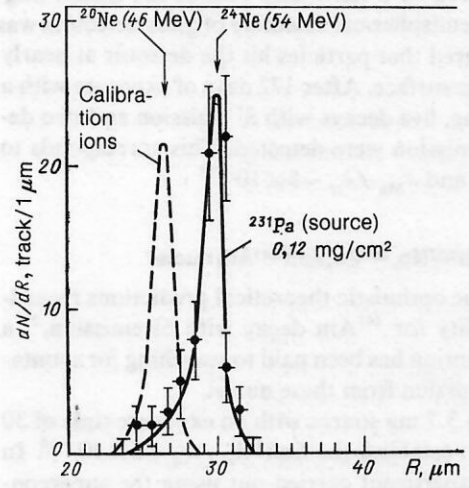

FIG. 9. Range distribution of clusters (^{24}Ne) detected in ^{231}Pa decay and of calibration ions (^{20}Ne).

over an area of 17 cm^2 was used. Lavsan detectors of thickness 170 μm for excluding contamination from α activity were located near the source with a clearance of about 0.1 mm. In these experiments, for reliable identification the tracks were detected in the angular range from 20 to 70° relative to the detector plane. Here the effective solid angle was ~60% of 2π. In order to decrease the cosmic-ray background the exposure was made under a shielding layer equivalent to 7 m of concrete. Two exposures of the detectors of duration 142 and 168 h allowed the detection of 12 and 13 Ne tracks, respectively.[12] The following three exposures raised the total number of Ne tracks to 55 (Ref. 14). Later,[15] a significantly thinner source containing 10 mg of matter over an area of 81 cm^2 was used, and after several exposures of total duration 103 days 197 decays with Ne emission were detected. The probability ratio obtained from all the experiments was $\lambda_{Ne}/\lambda_\alpha = (3.8 \pm 0.7) \times 10^{-12}$. The experimental charge resolution allowed Ne tracks to be distinguished from F tracks. However, none of the tracks could be attributed to fluorine. This implies that the probability for F yield is at least 100 times smaller than that for Ne yield.

In the experiments on ^{232}U decay carried out at Berkeley[13] a 0.5 mCi (~0.02 mg) source was used. It was surrounded by a track detector in the form of a Cronar hemisphere. The measurements were carried out in a vacuum over several months. Altogether 31 decays were detected, corresponding to a probability ratio of $\lambda_{Ne}/\lambda_\alpha = (2.0 \pm 0.5) \times 10^{-12}$. Geometry of the detector in the form of a hemisphere was chosen because for the track-identification technique developed at Berkeley it was necessary to ensure that the particles hit the detector at nearly normal incidence.

Experiments with ^{233}U, ^{234}U, ^{235}U, and ^{236}U nuclei

It is important to trace the dependence of the cluster spontaneous-emission probability on the mass number of the decaying nuclide for individual elements. In the case of radium this has been done for four isotopes. Five isotopes have been studied in the case of uranium, but the cluster-emission effect was detected only for the three lightest ones.

The data on ^{232}U were given above. The ^{233}U nucleus was studied in Ref. 16. The total amount of ^{233}U was 75 mg (0.75 mCi). The thickness of the layer was 0.33 mg/cm^2. A polyethylene terephthalate detector of thickness 170 μm was located along the uranium layer with a gap of ~1 mm, and the entire installation was screened by cadmium to shield it from thermal neutrons. The exposure time was 28 days. Altogether 16 neon tracks were detected, which gives $\lambda_{Ne}/\lambda_\alpha = (7.5 \pm 2.5) \times 10^{-13}$. This result has been confirmed by measurements carried out at Berkeley.[17] In these measurements the hemispherical assembly of Cronar layers was exposed in a vacuum for 6 months to a ^{233}U source of strength 0.1 mCi (~10 mg). The result $\lambda_{Ne}/\lambda_\alpha = (5.3 \pm 2.3) \times 10^{-13}$ is in good agreement with the results of Ref. 16. In Refs. 18 and 19 an attempt was made to study ^{233}U decay with ^{24}Ne emission by the method used in Ref. 2 and by a radiochemical method. However, in spite of the great effort that was made the sensitivity proved to be insufficient, and only an upper limit of $\lambda_{Ne}/\lambda_\alpha < 9.5 \times 10^{-13}$ was established. We note that this limit is close to the level of the effect obtained in Refs. 16 and 17. In connection with obtaining data on ^{232}U and ^{233}U decay, study of ^{234}U decay is quite interesting. There are several reasons for this.[20]

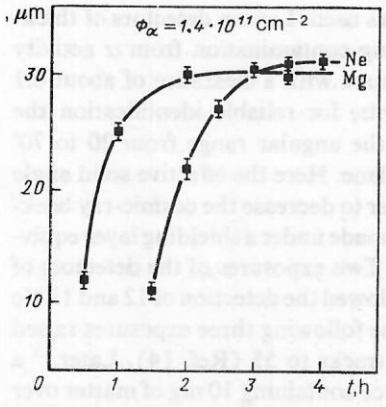

FIG. 10. Dependence of the length of etched tracks of neon and magnesium from ^{234}U decay on the etching time.

Experiments on spontaneous cluster emission by ^{234}U nuclei have been carried out at Berkeley[21] and at Dubna.[22] Both groups discovered decay with emission of both Ne and Mg. In Ref. 21 roughly 11 decays with Ne emission and three decays with Mg emission were detected, while in Ref. 22 for an exposure time of 2 days these numbers were 31 and 16, respectively. For identifying Ne and Mg clusters, in addition to the usual technique of comparison with the calibration curves v_t/v_m (R_{res}) (see the above discussion of Fig. 8), the difference between the dependences of the etched track length on the etching time for Ne and Mg was used (Fig. 10). This difference can be seen more clearly in Fig. 11a, where we give photomicrographs of Ne and Mg tracks after 3.5 hours of etching. Later the Berkeley group improved the statistics, and in Ref. 23 data on 108 and 36 cases of Ne and Mg emission, respectively, were given. The relative probabilities $\lambda_{cl}/\lambda_\alpha$ are $(3.9 \pm 1.0) \times 10^{-13}$ for Ne and $(2.3 \pm 0.7) \times 10^{-13}$ for Mg according to the data of Ref. 22, in good agreement with the data of Refs. 21 and 23.

Cluster emission by the heavier uranium isotopes ^{235}U and ^{236}U has also been studied in Ref. 22. However, only upper limits on the relative probability $\sim 10^{-11}$–10^{-12} were obtained there.

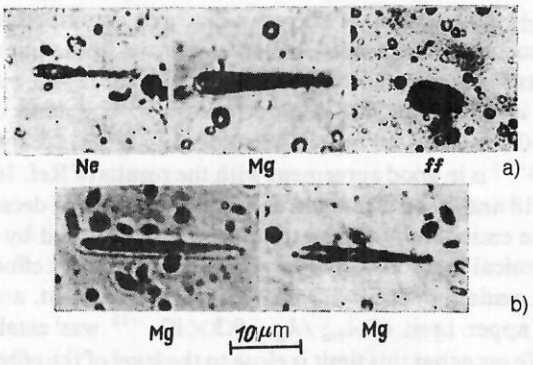

FIG. 11. Photomicrographs of cluster tracks: a—neon, magnesium, and fission fragments (*ff*) from ^{234}U decay; b—magnesium from ^{236}Pu decay.

The experimental spontaneous cluster-emission probabilities for the two even–even isotopes of uranium ^{232}U and ^{234}U fit nicely into a systematics similar to the Geiger–Nuttall systematics for α decay (see Sec. 5 below). A similar conclusion regarding Ra isotopes was drawn earlier in Refs. 7, 24, and 25.

Experiments with ^{230}Th and ^{232}Th nuclei

In the experiment of Ref. 26, carried out at Dubna with a source containing 210 mg of ^{230}Th mixed with 310 mg of ^{232}Th and having an area of 1040 cm^2, after 64 days of measurements 165 Ne ion tracks were obtained. It was shown that all of these are associated with the decay of the ^{230}Th nucleus. The relative probability for this process is $(5.6 \pm 1.0) \times 10^{-13}$. In the experiments carried out at Berkeley[17] with a thick ^{232}Th source of area 77 cm^2 over a period of 10 months, no cluster tracks were detected. Here $\lambda_{cl}/\lambda_\alpha < 5 \times 10^{-11}$. We note that the sensitivity of searching for clusters in these experiments and in the experiments with ^{235}U (Ref. 22) corresponded to periods of $\sim 10^{20}$–10^{21} yr, which is close to the experimentally determined limit for spontaneous fission of ^{232}Th ($\sim 10^{21}$ yr) (Ref. 27).

Experiments with ^{236}Pu and ^{238}Pu nuclei

Data on these isotopes are of considerable interest from the viewpoint of studying correlations between the cluster emission probability and the nuclear fissility parameter. In Ref. 28 the ^{236}Pu isotope was obtained by bombarding a ^{238}U target with protons of energy 30 MeV at the cyclotron of the Kurchatov Institute of Atomic Energy according to the following scheme: $^{238}\mathrm{U}(p,3n)^{236}\mathrm{Np} \xrightarrow{\beta^-} {}^{236}\mathrm{Pu}$. Altogether, 0.51 μg of Pu was extracted with isotope content 66% ^{236}Pu and 34% ^{238}Pu. During an exposure time of 689 days two Mg tracks were detected with energy of about 70 MeV. It was shown that they were associated with ^{236}Pu. The relative probability is $\lambda_{Mg}/\lambda_\alpha \sim 2 \times 10^{-14}$. In Fig. 11b we show photomicrographs of the two Mg ion tracks that were found.

Observation of cluster emission from ^{238}Pu is reported in Ref. 23. In working with this sample, serious difficulties arise, owing to the large background from spontaneous-fission fragments. To eliminate it, the detectors of phosphate glass were covered by a foil which retards the fission fragments. Here a hemispherical assembly of glass detectors was used which ensured that particles hit the detector at nearly 90° relative to the surface. After 172 days of exposure with a source of 10.5 mg, five decays with Si emission and two decays with Mg emission were detected. This corresponds to $\lambda_{Si}/\lambda_\alpha \sim 10^{-16}$ and $\lambda_{Mg}/\lambda_\alpha \sim 5 \times 10^{-17}$

Experiments with ^{237}Np, ^{240}Pu, and ^{241}Am nuclei

Owing to the optimistic theoretical predictions regarding the probability for ^{241}Am decay with Si emission,[29] a great deal of attention has been paid to searching for spontaneous cluster emission from these nuclei.

In Ref. 26 a 3.7 mg source with an exposure time of 30 days was used to establish the limit $\lambda_{cl}/\lambda_\alpha < 5 \times 10^{-15}$. In Ref. 11, in an experiment carried out using the superconducting spectrometer SOLENO, along with ^{14}C emission from ^{226}Ra, a limit on ^{34}Si emission from ^{241}Am of $\lambda_{Si}/\lambda_\alpha < 3 \times 10^{-12}$ was obtained. In Ref. 30 solid-state Lexan poly-

carbonate detectors were used to obtain the limit $\lambda_{cl}/\lambda_\alpha < 4.2\times10^{-13}$. The highest sensitivity was attained in Ref. 31. Using a source of mass 8 mg, after 6 months of exposure on phosphate glasses it was established that $\lambda_{cl}/\lambda_\alpha < 7\times10^{-16}$ for ^{241}Am.

The ^{237}Np nucleus was studied in Ref. 26. Not a single cluster track was detected using a source containing 320 mg of matter over an area of 500 cm^2 after 122 days of exposure. This corresponds to $\lambda_{cl}/\lambda_\alpha < 4\times10^{-14}$. At present, the ^{240}Pu nucleus closes the circle of nuclei which have been studied up to now. In Ref. 25 the limit $\lambda_{cl}/\lambda_\alpha < 1.3\times10^{-13}$ was established. A source of 230 μg/cm of total area 30 cm^2 was used. Measurements with a Cronar detector were carried out for 2 months.

In Table II we summarize the experimental results discussed in detail above. In cases where several measurements were carried out for the same decaying nucleus, we give the recommended mean values. These are used below for the theoretical analysis (see Table XI).

4. REVIEW OF THEORETICAL APPROACHES TO THE DESCRIPTION OF SPONTANEOUS CLUSTER EMISSION

The discovery of this new type of radioactivity raised the question of the position occupied by this phenomenon in the overall picture of nuclear physics. In order to answer this question it is necessary to understand the fundamental qualitative regularities of the process. It is natural to look for analogies by comparing this new phenomenon with the other two known types of radioactivity involving emission of composite particles: spontaneous fission and α decay.

Experimental and theoretical studies of the main features of fission unambiguously indicate that the nucleus undergoes strong rearrangement during its breakup into a pair of fragments of similar mass. In fact, experiment shows[35] that fission fragments i and j, emitted with a sizable probability, have average kinetic energy T_{ij} which is much smaller than the Coulomb interaction energy of these fragments at the contact point B_{ij}^{Coul} if it is assumed that they have the equilibrium shape. Here the energy yield of the process Q_{ij} proves sufficient for the Coulomb interaction energy $B_{ij}^{\text{Coul}}(B_i, B_j)$ to satisfy the condition

$$Q_{ij} \geqslant B_{ij}^{\text{Coul}}(\beta_i, \beta_j) + \Delta E_i^{\text{def}}(\beta_i) + \Delta E_j^{\text{def}}(\beta_j),$$

in some range of fragment deformation parameters β_i and β_j larger than or equal to their equilibrium values β_i^0 and β_j^0. Here

$$\Delta E_{i(j)}^{\text{def}} = E_{i(j)}^{\text{def}}(\beta_{i(j)}) - E_{i(j)}^{\text{def}}(\beta_{i(j)}^0),$$

where $E_{i(j)}^{\text{def}}(\beta_{i(j)})$ is the deformation energy of the fragment $i(j)$ corresponding to the value $\beta_{i(j)}$. Therefore, for strongly prolate fragment states the process of their emission is an above- or near-barrier process. In the limiting case of cold fission $Q_{ij} \approx T_{ij} \approx B^{\text{Coul}}(\beta_i^0, \beta_j^0)$, but the relative probability for such fission is very small. From the theoretical point of view the nucleus can split into a pair of deformed (or, in exceptional cases, spherical) fragments if it is strongly prolate (with deformation parameter more than twice as large as the equilibrium value) before the breakup. The stage corresponding to the transition to this state is described in the language of collective models taking into account shell corrections using the important assumption that the deformation is adiabatic relative to the one-particle motion. The actual breakup, which is nonadiabatic, leads mainly to the formation of strongly excited fragments with excitation energies $E_{i(j)}^* \geqslant \Delta E_{i(j)}^{\text{def}}$.

The phenomenon of α decay differs fundamentally from fission in that the energy release Q_α in the breakup of the parent nucleus A_i into an α particle and a daughter nucleus A_f is always significantly smaller than the height of the Coulomb barrier $B_{\alpha A_f}^{\text{Coul}}$, and the daughter nucleus is formed in the ground state or in a weakly excited state, i.e., this is a sub-barrier nonadiabatic process without significant rearrangement of the parent nucleus. The latter property indicates that α decay is similar to direct nuclear reactions with cluster transfer or knockout, for which the reduced probability is determined by the value of the corresponding shell spectroscopic factors.

In nuclear decay with emission of a heavy cluster X ($X = {}^{14}$C, ^{24}Ne, ^{28}Mg, ^{32}Si), as in α decay, the relation $Q_X < B_{XA_f}^{\text{Coul}}$ is preserved, i.e., the process is deeply sub-barrier. Experiment (see above) shows that the energy of the emitted fragments is $E_X^{\text{exp}} \simeq Q_X(A_f/A_i)$, so that the daughter nuclei and clusters are practically unexcited. Both of these arguments indicate that no significant rearrangement of the parent nucleus can occur in the decay process, and that decay with heavy-cluster emission can be an analog of α decay. However, we note that as the mass A_X of the emitted cluster X increases, the value of the corresponding ratio $Q_X/B_{XA_f}^{\text{Coul}}$ also increases, so that in the end a transition to the "fission" mechanism must occur. The question of the range of masses A_X where this transition occurs and the probabilities for processes in the transition region is still unanswered.

Let us first consider the theoretical approaches to the description of cluster decay based on various modifications of the superasymmetric-fission model.

Spontaneous cluster emission as a special type of fission

The theoretical schemes which treat cluster decay as a form of fission are based on the following assumptions:

1. Collective variables characterizing the shape of the decaying system are introduced.

2. It is assumed that the motion in these variables is adiabatic relative to the one-nucleon motion.

3. It is assumed that the decaying system is described by the Schrödinger equation for the collective variables. The one-dimensional equation or the equation with separable variables is used.

4. The potential for the cluster–residual-nucleus interaction in the external region is constructed.

5. The interaction potential in the internal region is constructed using a phenomenological or theoretical approach.

6. The dependence of the inertia parameters on the collective variables is determined.

7. The system in the form of a cluster plus a residual nucleus is viewed as a pair of unexcited particles detected in the exit channel.

8. The energy of the system, defined as the difference between the total energy in the initial state (including the energy of the lowest vibrational level in the constructed potential) and the total internal energy of the fragments, is set equal to the energy yield Q.

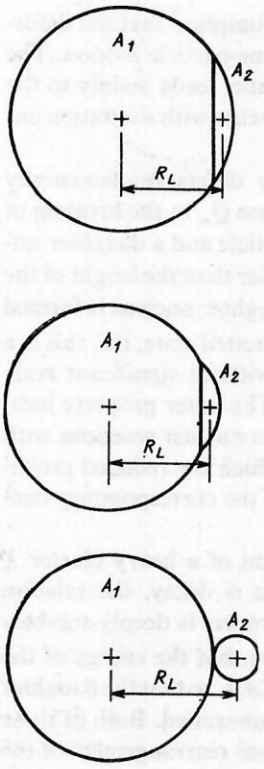

FIG. 12. Evolution of the system in the collective variable R_L (Ref. 36).

As an example of an approach of this type, let us consider the model which is most highly developed in this regard.[36] It is assumed that the fission process occurs as shown in Fig. 12, where the plane divides the system in such a way that the masses of the fragments to the right and to the left of it correspond to the masses of the particles in the exit channel. The variable R_L corresponds to the distance between the centers of mass of these segments. The surface of the cluster (and the corresponding segment) is assumed to be spherical. The quadrupole and hexadecapole deformation of the parent and daughter nuclei are taken into account. Here

$$R_L = \sum_i c_i \left[R_i + d_i + \frac{3}{4} \frac{d_i^2}{R_i + d_i} \right], \tag{1}$$

where the variables that we use are defined in Fig. 13. The value of c_i is determined in terms of the cross-section radius ρ_c:

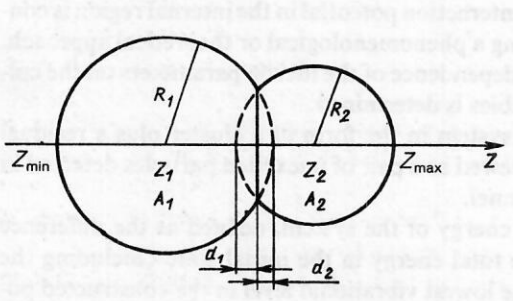

FIG. 13. Definition of the parameters in Ref. 36.

$$\rho_c^2 = c_i^{-1} [R_i^2 - (R_i - d_i)^2]. \tag{2}$$

The rule for the change of shape of the nucleus from the parent to the daughter nucleus is, in principle, not determined. Therefore, it is assumed that the c_i vary as

$$c_i = c_i^{(f)} + (c_i^{(i)} - c_i^{(f)}) (d_i/d_0)^{s_i}, \tag{3}$$

where d_0 is the maximum value of d_i; $c_i^{(i)}$ and $c_i^{(f)}$ are the initial and final values of the semiaxis of the ellipsoid determining the shape of the nucleus; s_1 and s_2 are free parameters. Minimization of the action imposes rather rigorous conditions on s_1 and s_2, and the dependence of the result on them turns out to be weak.

The interaction of the particles beyond the contact point is described by the Coulomb potential for the repulsion of an ellipsoid and a sphere. The dimensional parameter of the nucleus r_0 is taken to be 1.20 F. At small distances the interaction is parametrized as

$$V(R_L) = -E_v + (E_c + E_v - Q) f(k, p); \tag{4}$$

$$f(k, p) = (1 + k) p^2 - kp^3, \tag{5}$$

where Q is the decay energy, E_c is the Coulomb energy at the fragmentation point, $R_L = R_L^p$, $p = (R_L - R_L^{(i)})/(R_L^{(p)} - R_L^{(i)})$; $E_v = (\hbar/2)\sqrt{C/M_0}$ is the zero-point energy in the coordinate R_L, taken in the harmonic approximation, $C = 2V(R_L)/(R_L - R_L^{(i)})^2$ is the stiffness coefficient, and M_0 is the value of the mass parameter at the initial point. The values of the parameter k were chosen from calculations of the energy of the system in the form described above using the liquid-drop model.

The same model was also used to obtain the inertia parameter, which determines the relation between the kinetic energy T and the speed of motion in the collective coordinate R_L:

$$M = 2T/\dot{R}_L^2, \tag{6}$$

where the model without vortex motion and without overflow of the liquid from the volume A_1 to A_2 was used. The quantum corrections to the effective mass M were not included.

The sensitivity of the results to the choice of model parameters was kept under control.

The results are compared with experiment in Table XI. The results obtained using this approach are in good agreement with experiment. A significant part of the rms deviation of the results can be attributed to the absence of even–odd effects in this scheme. A small systematic underestimate of the width of transitions from even–even nuclei is observed. Calibration of the results (a fit of k) to the decay of even–even nuclei would lead to an improvement of the agreement.

Reference 37 differs from Ref. 36 in the choice of collective variables and mass parameters. Here we use the usual set of deformation parameters α_2, α_3, α_4. The configuration at the contact point (Fig. 12) is not described by these parameters, and therefore it was assumed that the transition is realized at it when the lowest moments of the density distribution function of the deformed system and of the contact configuration coincide.[36] The state of the initial system was determined by the procedure of minimizing the deformation

potential energy calculated using the shell-correction method.[39] From this one can also determine the stiffness coefficients C_λ in all the deformation modes:

$$C_\lambda = \frac{\partial^2 V(\{\alpha^2\})}{\partial \alpha_\lambda^2}. \quad (7)$$

The fluctuations leading to the decay are assumed to be harmonic. The decay probability is assumed to be equal to the product of the probability for the formation of the needed configuration in the surface-oscillation process W_f and the usual Coulomb penetration factor P_f with cutoff radius given by the parameter $r_0 = 1.2$ F. The mass parameters B_λ were calculated in the liquid-drop model, but the same phenomenological factor k for all nuclei was inserted into the expression for the oscillation frequency:

$$\omega_\lambda = k\sqrt{C_\lambda/B_\lambda}, \quad (8)$$

with k found to be 0.35 from a fit to the experimental width of the decay $^{223}\text{Ra} \rightarrow {}^{14}\text{C}$. The decrease of the fragment formation probability W_f due to this apparently effectively takes into account the fact that the formation of a configuration of two nuclei in contact with each other from a system with similar lowest moments occurs with a certain (very small) probability.

Except for the case of Ra isotopes, the numerical results of Ref. 37 pertain to cases where there are no experimental data. Good agreement is observed for ^{223,226}Ra, while in the other two isotopes the calculated width is roughly two orders of magnitude too high. The general tendency for the decay width to decrease with increasing cluster mass is considerably stronger than in Ref. 36.

One deficiency of these studies[36,37] is the use of a purely Coulomb interaction in the external region. Here the shape of the potential barrier does not allow the description of near-barrier scattering and reactions with ions corresponding to the exit channel of the decay. For example, for the cutoff parameter at $r_0 = 1.2$ F, its height in the $^{14}\text{C} + \text{Pb}$ channel is roughly 10 MeV larger than the experimental value. In principle, the inclusion of the nuclear interaction of the fragments tends to increase the penetration factor. References 40 and 41 are free from this defect, since there the interaction in the external region is described by a "proximity" potential.[42] The deformation of the parent nucleus was taken into account in a later study,[41] as in Refs. 36 and 37, and the possibility of decay in a direction not coinciding with the symmetry axis was allowed. The collective variable L used in Refs. 40 and 41 was defined as the distance between the farthest separated points of the system (Fig. 14) in the direction of θ. The interaction potential in the external region was chosen to have the form

$$V(L, \theta) = M_1 + M_2 - M + V_c + V_p, \quad (9)$$

where M, M_1, and M_2 are the masses of the parent and daughter nucleus and the cluster, and V_c and V_p are the Coulomb and "proximity" potentials, respectively. In the internal region

$$V(L, \theta) = a(L - L_0)^\nu, \quad (10)$$

where L_0 is the dimension of the initial nucleus in the direction of θ, and a and ν are parameters determined from the requirement that the potential curves (9) and (10) join smoothly at the contact point.

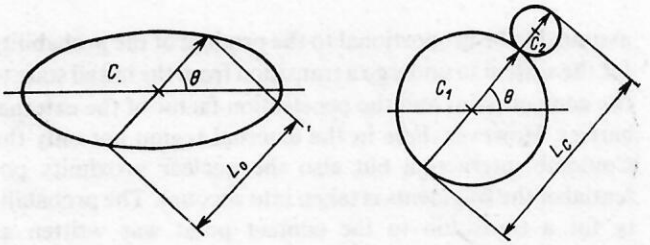

FIG. 14. Definition of the variable L at the initial point L_0 and at the contact point L_C from Ref. 41.

The mass parameter in that study was set equal to the reduced mass. The quadrupole oscillation period of the initial nucleus was treated as a parameter calculated from the experimental data. It had two values:[41] $\tau = 5\times10^{-23}$ sec for even–even nuclei and $\tau = 5\times10^{-21}$ sec for odd nuclei. Both studies,[40,41] especially the second, obtained very good agreement with experiment (see Table XI), but no explanation was found in those studies for the large frequency difference (corresponding to the oscillation energies $\hbar\omega_{ev} = 15$ MeV and $\hbar\omega_{odd} = 0.15$ MeV). As we shall see below, this indicates the presence of effects unrelated to barrier penetration.

A simpler form of the potential barrier was used in the series of studies of Refs. 29, 43–45, 47, and 48. The studies of Refs. 43–45, carried out right after the discovery of cluster radioactivity, contained the first theoretical response to the experimental results.[1,2] In this approach in the external region $R > R_{cont}$ the interaction is taken to be a point Coulomb interaction of the decay fragments, while in the region where the fragments overlap it is approximated by an expression like (5), neglecting the cubic term. The value of the potential in the initial state is assumed to be Q_X. The mass parameter corresponds to the reduced mass of the clusters. The free parameter is taken to be the zero-point energy E_V, which, in turn, in the most refined versions of the fits[29,47] is written as

$$E_V^X = \begin{cases} Q_X(ax^2+bx+c), & 4 < A_X < \tilde{A}_X, \\ Q_X c, & A_X > \tilde{A}_X, \end{cases}$$

where $x = (A_X - 24)/20$. The parameters a, b, c, and A_X are selected separately for even–even, odd–even, etc., parent nuclei. The exponential sensitivity to E_V^X is achieved artificially[43,44] by adding the energy E_V^X to Q_X when calculating the barrier penetration factor. The theoretical cluster decay width is set equal to the product of the pre-exponential factor $\hbar/2E_V^X$ and the penetration factor of the assumed barrier, calculated semiclassically.

As can be seen from Table XI, by careful selection[47] of more than 12 parameters it is possible to obtain good agreement with the experimental data. However, comparison with earlier fits[43,44] and even with that of Ref. 29, where calculations were carried out for several thousand possible variants of cluster emission, shows that, at least in the earlier versions of this theoretical approach, the predictive power of this approach is limited and requires correction of the model parameters to include the more complicated structure of the cluster and the parent nucleus.

An important step in the development of "fission" schemes for describing cluster radioactivity was made in Ref. 50. As in Ref. 37, the decay probability per unit time is

assumed to be proportional to the product of the probability for the system to undergo a transition from the initial state to the contact point and the penetration factor of the external barrier. However, here in the external region not only the Coulomb interaction but also the nuclear proximity potential of the fragments is taken into account. The probability for a transition to the contact point was written as $P_0(A_1) \equiv W_f$ from Ref. 37:

$$P_0(A_1) = |\psi_R(A_1)|^2 \sqrt{B_{\eta\eta}(A_1)} \frac{200}{A},$$

where $B_{\eta\eta}(A_1)$ is the mass parameter of the system, computed, as in Ref. 36, using the hydrodynamical model; $\eta = (A_1 - A_2)/(A_1 + A_2)$ is a collective variable chracteristic of fragmentation theory. The function $\psi_R(\eta)$ is the solution of the Schrödinger equation

$$\left[-\frac{\hbar^2}{2\sqrt{B_{\eta\eta}}}\frac{\partial}{\partial\eta}\frac{1}{\sqrt{B_{\eta\eta}}}\frac{\partial}{\partial\eta} + V(\eta, R)\right]\psi_R(\eta) = E_R\psi_R(\eta)$$

in the variable η, where the distance R is treated as a parameter. In the present study its specific value is chosen to be the distance at the contact point. The potential $V(\eta, R)$ at this point was chosen to be equal to the external potential. Reference 50 gives good results for the ^{14}C cluster, but there is a tendency for the cluster radioactivity widths to vary differently from experiment: the ratio λ_X/λ_α increases with increasing X. Unfortunately, it is difficult to figure out the possible reasons for this from the brief article of Ref. 50. Earlier studies of this group were devoted, like Ref. 6, to seeking the optimal variants of the decay by constructing potential surfaces $V(\{\eta\}, R)$ (where $\{\eta\}$ is understood as some set of variables from fragmentation theory, including, of course, η) and do not claim to describe the phenomenon quantitatively (see, for example, Ref. 49).

Several other versions of the two-body barrier used for theoretical calculations of cluster-radioactivity processes are given in the literature.[51]

Summarizing the results on the theoretical study of cluster decay using models of superasymmetric fission, we note that, in spite of the differences between these schemes, all these models give a fairly accurate description of the experimental data for this quite complicated, little-studied process. Serious discrepancies between the theoretical and experimental results arise only in the case of predictions. However, the agreement between theory and experiment should not be considered proof of the validity of the initial premises of fission-type models, since each realization of this scheme neglects certain physically obvious features. First of all, it is necessary to include the zero-point energy correctly. In the studies where this was not done, $E_V = 0$, inclusion of this energy tends to change the results by two orders of magnitude. Second, almost all these studies (except for Refs. 40, 41, and 50) use a purely Coulomb form of the fragment interaction potential in the external region, which strongly contradicts the data on the cross sections for cluster elastic scattering on these nuclei. Inclusion of the nuclear interaction near the maximum of the potential barrier, which makes its shape consistent with the scattering data, drastically (by several orders of magnitude) raises the barrier penetration factor. Third, in these studies the behavior of the potential curve in the internal region is determined purely phenomenologically from the cluster radioactivity width (except in Ref. 36, where, however, a not very reliable parametrization of the liquid-drop model is used), which introduces a large uncertainty into the result. Fourth, the introduction into the equation of motion of an inertial parameter in the collective coordinate different from the reduced mass in those studies where this parameter was neglected tends to lower the barrier penetration factor by up to two orders of magnitude, depending on the cluster mass. Finally, the scheme of adiabatic deformation of the nuclear surface is fundamentally incapable of describing the breakup of a nucleus into two fragments with fixed mass and internal state—the specification of the shape of the surface results in a broad spectrum of fragments of various masses and excitation energies. Although this approach is justified for studying nuclear fission, where such a fragment spectrum does actually arise, it is difficult to apply it to decay processes, where the fragments in the final state are strictly determined. Their weight in the spectrum is very small, so that a simple adiabatic calculation can raise the cluster formation probability in the pre-barrier region by several orders of magnitude. However, we should make it completely clear that this does not imply that an adiabatic mechanism of cluster formation cannot be realized in the cases of heavy decay which have been studied. For example, the results of Ref. 36 can be affected only by the inclusion of the second, third, and fifth items listed above. Here the choice of the potential in the internal region is quite well justified, and the other two factors can to a significant degree cancel each other.

Systematics of the experimental data as a source of information about the cluster decay mechanism

In view of the successes and problems of fission-type models discussed above, to understand the cluster decay mechanism it is useful to carry out a direct analysis of the full set of experimental data. Moreover, such an analysis can give phenomenological estimates of the decay probabilities needed for planning new experiments. With models of superasymmetric fission in mind, let us consider Fig. 15, where we give the logarithms of the cluster decay periods $T^{cl}_{1/2}$ together with the periods $T^{s.f}_{1/2}$ for spontaneous fission for the U and Pu isotope chains as functions of the fissility parameter Z^2/A. We see that, whereas the dependence $T^{s.f}_{1/2}$ is bell-shaped, the periods $T^{cl}_{1/2}$ fall off sharply with increasing Z^2/A for a given isotope chain. In our opinion, a more important feature is that the ratios $T^{cl}_{1/2}/T^{s.f}_{1/2}$ are not constant, but increase sharply with increasing Z of the parent nucleus. This might indicate that if the cluster decay mechanism is similar to ordinary fission, the deformation barriers and trajectories in the deformation space for these two processes differ significantly (see below for a more detailed discussion of this point). Moreover, from a purely practical point of view the systematics of the periods $T^{cl}_{1/2}$ as a function of Z^2/A is inconvenient for making estimates and predictions, since the points for one type of emitted cluster but different Z of the parent nuclei do not lie on the same curve. Let us therefore consider the technique used for the α-decay systematics.

The very simple model of a decaying nucleus proposed

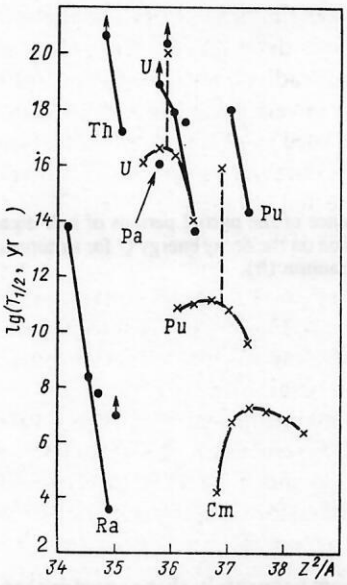

FIG. 15. Dependence of the logarithms of the partial periods of spontaneous fission (crosses) and cluster decay (black circles) on the fissility parameter Z^2/A.

in 1928 by Gamow for describing α decay was used in the pioneering studies of Refs. 1 and 2 and also in later studies[7,23] for a preliminary analysis and extrapolation of the experimental data. In this model a pointlike structureless cluster with frequency $\nu_{\rm cl}$ oscillates in a square well of radius

$$R_k = r_0'(A_X^{1/3} + A_f^{1/3}), \qquad \text{(A)}$$

separated from the external region by a Coulomb barrier. The half-decay period is written as

$$T_{1/2}^{\rm cl} = \ln 2/2\nu_{\rm cl} P_L^{\rm cl}, \qquad (11)$$

where the barrier penetration factor $P_L^{\rm cl}$ for a cluster of angular momentum L and decay energy Q_X is defined as

$$P_L = \exp(-K_L), \qquad (12)$$

while for $L = 0$ (Ref. 52)

$$K_0 = \frac{2}{\hbar}\sqrt{\frac{2\mu}{Q_X}}\, Z_1 Z_2 e^2 [\arccos\sqrt{y} - \sqrt{y-y^2}]. \qquad (13)$$

Here $y = Q_X R_k/Z_1 Z_2 e^2$, $\mu = A_1 A_2/(A_1 + A_2)$, and the indices 1 and 2 label the charge (mass) of the cluster and the daughter nucleus.

In Fig. 16, taken from Ref. 28 with the addition of more recent data, we show the dependence of log $T_{1/2}^{\rm cl}$ on K_0, which according to (11) and (12) should be linear for each type of emitted cluster. For methodological reasons, in the same figure we give the corresponding dependence for favored α transitions in the parent nuclei in question. We see that for all types of emitted ions, including α particles, the experimental data for even–even nuclei tend to lie on straight lines of roughly the same slope. The exception, as in the case of α emission, is the cluster decay of the odd parent nuclei ^{223}Ra, ^{231}Pa, and ^{233}U whose periods deviate from the systematics for even–even nuclei. The even–odd effect is illustrated in more detail in Fig. 17 for the Ra and U isotope chains. On the horizontal axis we give the value of $(Q_X)^{1/2}$ in terms of which log $T_{1/2}$ is expressed in the classical Geiger–Nuttall relation for α decay:

$$\lg T_{1/2} = A(Z) + B(Z)/Q_X^{1/2}. \qquad (14)$$

We note that in the case of α decay the scale of even–even effects depends on the type of α transition, and for favored transitions it is significantly smaller[53] than in Fig. 17.

Therefore, the dependence on the decay energy and on the characteristics of the Coulomb barrier for cluster emission is of the same nature as for α decay, but the cyclic frequencies whose values according to (11) and (12) determine the intersection points of the straight lines with the vertical axis in Fig. 16 depend exponentially on the cluster mass.

We note that if the parameter r_0 is not restricted by the physically reasonable condition that at the contact point of the decay fragments the value of R_k be no less than the sum of the experimental fragment radii, i.e., if we take $r_0 \geqslant 1.2$ F and use r_0 as a fitted parameter, then, as was shown in Ref. 23, all cases of the cluster decay of even–even nuclei (except for α decay) lie on a single line ($r_0 = 0.928$ F, $\nu_{\rm cl}^{\rm ev,ev} = 4.3\times10^{26}$ sec^{-1}). This representation of the data is convenient for making estimates and for interpolation, but it should be borne in mind that the unphysical choice of cutoff radius of the Coulomb potential R_k implicity mimics the dependence of the pre-exponential factor in (11) on the cluster mass. (See Ref. 54 for a more detailed discussion of this question.) In a more serious treatment of the value and mass dependence of the parameter $\nu_{\rm cl}$, it is necessary to take into account the fact that the potential barrier of the decaying nucleus is formed by the sum of the Coulomb potential $V_{XA_f}^{\rm Coul}$ and the nuclear potential $V_{XA_f}^{\rm nucl}$ of the nuclei describing the interaction of the decay fragments. This program was realized in Ref. 56 using the Gamow model[46] with the nuclear interaction $V_{XA_f}^{\rm nucl}$ chosen phenomenologically. Here the

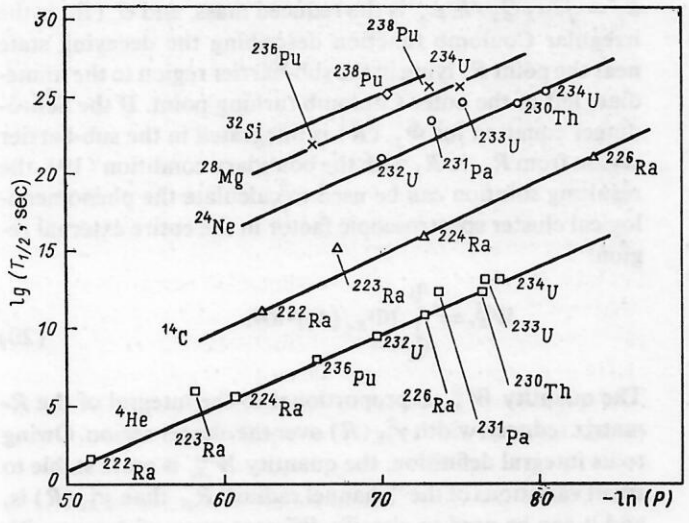

FIG. 16. Dependence of the logarithms of the partial periods of cluster decay on the natural log of the Coulomb-barrier penetration factor.

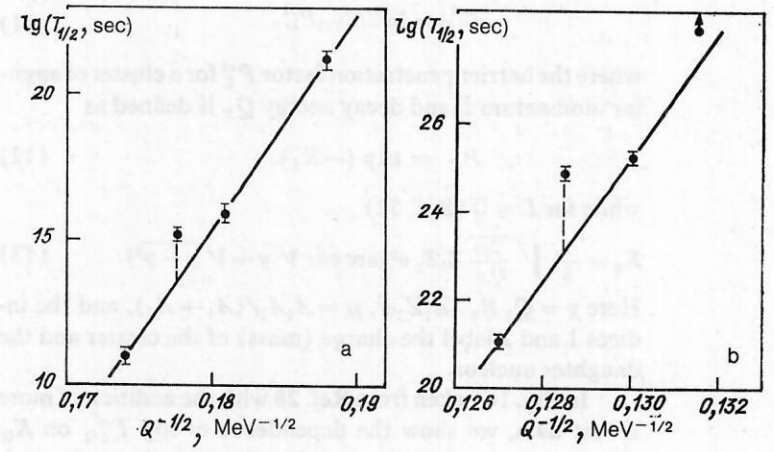

FIG. 17. Dependence of the partial periods of half-decay with cluster emission on the decay energy Q for isotopes of radium (a) and uranium (b).

width Γ_X for decay with emission of a cluster X was written as

$$\Gamma_X = \Gamma_X^{\text{Gam}} S_X, \tag{15}$$

where S_X is a spectroscopic factor determining the probability for forming the pair cluster X + daughter nucleus A_f, and Γ_X^{Gam} is the width describing the probability that the cluster penetrates the barrier:

$$\Gamma_X^{\text{Gam}} = \frac{\hbar v_X}{2R_{\text{in}}} P_X. \tag{16}$$

Here v_X is the cluster velocity, which in Ref. 56 was determined from the condition $\mu_X v_X^2/2 = 25A_X$ MeV. In contrast to (12) and (13), the penetration factor P_X is calculated numerically in the form of a standard semiclassical integral, with the lower limit equal to P_{in}, the inner turning point.

The phenomenological spectroscopic factors S_X were obtained in Ref. 56 using (15) and (16) from the experimental data on the cluster decay probabilities. They can be accurately approximated by the simple expression

$$S_X = (S_\alpha^{\text{ev.ev}})^{(A_X-1)/3}, \tag{17}$$

where $S_\alpha^{\text{ev,ev}} = 6.3\times10^{-3}$ for even–even parent nuclei and $S_\alpha^{\text{odd}} = 3.2\times10^{-3}$ for odd nuclei. We note that the values of S_α are close to the experimental results for the spectroscopic factors of favored α transitions in even–even and odd parent nuclei.[53] Relation (17) is in good qualitative agreement with the dependence of the parameter ν_{cl} on the cluster mass, shown in Fig. 16.

The authors of Ref. 57 proposed a different parametrization of the spectroscopic factor S_X, based on the thermodynamical approach. It is assumed that the probability for forming the system cluster + residual nucleus has the form

$$S_X \sim e^{-Q_X/T}, \tag{18}$$

where the "temperature" $T = \sqrt{Q_X/a}$ is expressed in terms of the single-particle level-density parameter a, chosen to be $a = A_f/8.0$ and $a = A_f/9.5$. In Table XI we give the first variant, which agrees best with experiment.

Therefore, in any model of the Gamow type using a realistic barrier shape one obtains spectroscopic factors for the emitted particle which are considerably smaller than unity and fall off rapidly with increasing particle mass. The natural question arises of how accurately these spectroscopic factors can be extracted from experiment. Reference 58 is devoted to a detailed study of this question. Let us briefly consider its main results.

Let us more rigorously define the concept of the external asymptotic cluster region of the parent nucleus, where it can be viewed as a set of fully formed decay products—the cluster and the daughter nucleus. The estimates made in Ref. 53 show that for α decay the inner limit of the asymptotic region can be taken to be $R_{\text{cl}} = 1.2(A_\alpha^{1/3} + A_f^{1/3})$F. Using the analogous definition for the case of cluster decay, in this region we define the phenomenological form factor of the cluster X in the decay channel c as the solution of the Schrödinger equation with potential $V_{XA_f}^{\text{nucl}}(R) + V_{XA_f}^{\text{Coul}}(R)$ coinciding with the real part of the optical potential describing the elastic scattering of the particle X on the daughter nucleus and with the boundary condition

$$\Phi_{Xc}(R) \to \sqrt{\frac{\hbar\Gamma_{Xc}k_c}{Q_X}}\, G_c(R), \tag{19}$$

where Γ_{Xc} is the experimental width of the decay with emission of the cluster X into the channel c ($c \equiv J_f$, σ_f, L), $k_c = \sqrt{2\mu_X Q_X}/\hbar$; μ_X is the reduced mass, and $G_c(R)$ is the irregular Coulomb function describing the decaying state near the point R_1 lying in the sub-barrier region to the immediate left of the outer Coulomb turning point. If the Schrödinger equation for $\Phi_{Xc}(R)$ is integrated in the sub-barrier region from R_{cl} to R_1 with the boundary condition (19), the resulting solution can be used to calculate the phenomenological cluster spectroscopic factor in the entire external region:

$$W_{Xc}^{\text{cl}} = \int_{R_{\text{cl}}}^{R_1} [\Phi_{Xc}(R)]^2\, dR. \tag{20}$$

The quantity W_{Xc}^{cl} is proportional to the integral of the R-matrix reduced width $\gamma_{Xc}^2(R)$ over the cluster region. Owing to its integral definition, the quantity W_{Xc}^{cl} is more stable to small variations of the "channel radius" R_{cl} than $\gamma_{Xc}^2(R)$ is, and it can be used to classify different types of decays with emission of particles X. In contrast to α decay, where the nuclear potential describing the α-particle interaction with the daughter nucleus $V_{\alpha A_f}^{\text{nucl}}(R)$ has been thoroughly studied throughout the entire cluster region, the problem of the in-

teraction of a heavy ion and a heavy nucleus at distances close to the inner boundary of the cluster region is at present far from a definitive solution.

In the current literature one can find numerous and very diverse versions of phenomenological potentials $V^{\text{nucl}}(R)$ describing elastic scattering, the reaction cross sections, and other inelastic processes for the interaction of composite particles with nuclei. This diversity is a consequence of the well-known discrete and continuous ambiguities of extracting the phenomenological potential parameters in the inverse scattering problem. The former arises when potentials differing in the number of bound states give a qualitatively similar description, and the latter arises when the data are described by potentials from a single discrete class which have different parameter sets (for example, ambiguities of the deep–narrow or shallow–wide type). The situation gets worse when a channel with strong absorption is studied. The experimental errors also significantly affect the results of solving the inverse problem.

Nevertheless, the ambiguities in the potentials for d, t, ^{3}He, and α particles interacting with nuclei can be eliminated by accurate study of the scattering of the corresponding particles at sufficiently high energy in a wide range of angles.[59] Rainbow scattering is no less informative in this sense.[60] Constraints on the parameters of potentials describing α-particle interactions with heavy nuclei are obtained by analyzing the sub-barrier (n, α) reaction.[53] In the case of target nuclei which are not too heavy, for which investigations have been carried out by one of the methods described above, the properties of the potentials turned out to be uniform.

In the fit for a class of L-independent potentials, first of all, the depth of the real part of any of these potentials is $\sim 50\mu_X/m_N$ MeV, i.e., they all fall into the category of "deep." Second, the number of bound states of the cluster in such potentials is not less than the number of forbidden states of the cluster in the parent nucleus, i.e., these potentials are not inconsistent with the generalized Levinson theorem (see Ref. 53).

In the studied cases the fit of the experimental cross sections by L-dependent potentials does not lead to any significant improvement of the description, in spite of the considerable increase in the number of parameters; moreover, the uniqueness of choosing the parameters is lost. This is evidence in favor of a variant with an L-independent potential.

For heavier target nuclei it turns out to be difficult to obtain a data set sufficient for eliminating the ambiguities, owing to the exponential falloff of the scattering cross section at low energies and large angles. Also, for clusters X with mass $A_X > 4$, (n, X) processes with slow neutrons are not observed experimentally.

The versions of the phenomenological potentials V_{XA}^{nucl} for the interaction of nuclei with mass $A \sim 208$ with "light" heavy ions $^{12-14}$C, ^{16}O, etc., existing in the literature are designed to describe elastic scattering and certain reactions. Almost all of them have a depth V_0 of the order of several tens of MeV, i.e., they fall into the category of "shallow" potentials and do not contain any bound states. In spite of their outward differences, for a fixed pair of interacting nuclei they give quite similar values of the location and height of the barriers. Meanwhile, at small distances—to the left of the barrier maximum—the behavior of the potential curves begins to diverge significantly. We note that owing to the strong absorption, the elastic-scattering cross sections in a wide energy range turn out to be insensitive to the behavior of the real part of the potential at small distances R. This class of potentials is not suitable for describing deeply subbarrier processes, since, first, they have no bound states (they do not satisfy the generalized Levinson theorem) and, second, their left-hand slope is practically arbitrary, while the dependence of W_{Xc}^{cl}, which is proportional to the barrier penetration factor, on the form of this slope is very strong.

The potentials used to describe the near-barrier fusion of heavy ions are effective potentials which model the strong coupling between channels characteristic of this process, and therefore they do not have any direct relation to the potentials $V_{XA_f}^{\text{nucl}}(R)$ that we are considering, which are designed to describe a single elastic channel.

Therefore, for constructing an interaction model it is necessary to use certain theoretical schemes. A detailed analysis[58] of various theoretical schemes has shown that the most productive approach to constructing the potential $V_{XA_f}^{\text{nucl}}$ is that based on the convolution (folding) of nucleon–nucleon (or nucleon–nucleus) interactions with the known spatial nucleon-density distribution functions of the interacting nuclei. In addition, this approach has a certain microscopic justification.[61] In the literature one finds the use of both double folding potentials, obtained from expressions

$$V_{\text{II}}(\mathbf{R}) = \int \rho_{A_f}(\mathbf{r}_1)\, \rho_X(\mathbf{r}_2)\, V_{NN}(\mathbf{R} + \mathbf{r}_1 - \mathbf{r}_2)\, d^3r_1\, d^3r_2, \tag{21}$$

and unary potentials obtained by convolution of the nucleon–nucleus optical potential with the spatial density distribution of the cluster:

$$V_{\text{I}}(\mathbf{R}) = \int \rho_X(\mathbf{r})\, V_{N-\text{nucl}}(\mathbf{R} - \mathbf{r})^* d^3r. \tag{22}$$

The depth of the folding potential has an important dependence on the form of the bare V_{NN} (for the double case) or $V_{N-\text{nucl}}$ (for the unary case) interaction and can vary by tens of percent for heavy nuclei. Since here the experimental data do not permit any particular type of bare interaction to be distinguished, it can be said that folding potentials reproduce the exact potentials with some (though, perhaps, insufficient) accuracy. A scheme purporting to introduce corrections for exchange effects in the double folding procedure was proposed in Ref. 62. However, we note that in the cluster region of interest to us the exchange components of the interaction play a less important role.

The procedure for calculating the cluster spectroscopic factors W_{Xc}^{cl} was based on the experimental data of Table II and on the use of expressions (21) and (22) for the potential $V_{XA_f}^{\text{nucl}}(\mathbf{R})$. The nucleon density of the cluster in Eqs. (21) and (22) was taken from Ref. 63, and that for the daughter nucleus was taken from Ref. 64. The bare $V_{N-\text{nucl}}$ potential for the unary folding variant were taken from the following studies (see Table III): 1—Ref. 65; 2—Ref. 66; 3—Ref. 67. The potentials V_{NN} for the double folding variant were taken from: 4—Ref. 62; 5—Ref. 68; 6—Ref. 68; 7—Ref. 69. In addition, we used the deep phenomenological potential (8) from Ref. 55, which was also used in Ref. 56 to extract the experimental spectroscopic factors. In those cases where the

TABLE III. Cluster spectroscopic factors W_{Xc}^{cl} for various potentials.

Decay		Potential		
A_i	$X+A_f$	1	2	3
^{222}Ra	^{14}C + ^{208}Pb	$2.9\cdot10^{-10}$	$1.6\cdot10^{-8}$	$3.7\cdot10^{-8}$
^{223}Ra	^{14}C + ^{209}Pb	$3.1\cdot10^{-12}$	$1.8\cdot10^{-10}$	$4.0\cdot10^{-10}$
^{224}Ra	^{14}C + ^{210}Pb	$2.2\cdot10^{-10}$	$1.5\cdot10^{-8}$	$3.0\cdot10^{-8}$
^{226}Ra	^{14}C + ^{212}Pb	$0.82\cdot10^{-10}$	$6.6\cdot10^{-9}$	$1.2\cdot10^{-8}$
^{230}Th	^{24}Ne + ^{206}Hg	$2.2\cdot10^{-18}$	$1.2\cdot10^{-15}$	$3.2\cdot10^{-15}$
^{231}Pa	^{24}Ne + ^{207}Tl	$1.1\cdot10^{-19}$	$5.4\cdot10^{-17}$	$1.5\cdot10^{-16}$
^{232}U	^{24}Ne + ^{208}Pb	$7.1\cdot10^{-19}$	$3.3\cdot10^{-16}$	$9.6\cdot10^{-16}$
^{233}U	^{24}Ne + ^{209}Pb	$4.5\cdot10^{-20}$	$2.5\cdot10^{-17}$	$6.7\cdot10^{-17}$
^{234}U	^{24}Ne + ^{210}Pb	$7.8\cdot10^{-18}$	$5.1\cdot10^{-15}$	$1.2\cdot10^{-14}$
^{234}U	^{28}Mg + ^{206}Hg	$6.1\cdot10^{-22}$	$7.0\cdot10^{-19}$	$2.1\cdot10^{-18}$
^{236}Pu	^{28}Mg + ^{208}Pb	$2.0\cdot10^{-22}$	$1.9\cdot10^{-19}$	$6.7\cdot10^{-19}$

4	5	6	7	8
$1.8\cdot10^{-6}$	$6.0\cdot10^{-6}$	$1.6\cdot10^{-6}$	$2.2\cdot10^{-6}$	$1.7\cdot10^{-9}$
$2.2\cdot10^{-8}$	$7.1\cdot10^{-8}$	$1.9\cdot10^{-8}$	$2.7\cdot10^{-8}$	$1.5\cdot10^{-11}$
$1.9\cdot10^{-6}$	$6.3\cdot10^{-6}$	$1.5\cdot10^{-6}$	$2.3\cdot10^{-6}$	$8.9\cdot10^{-10}$
$9.2\cdot10^{-7}$	$3.2\cdot10^{-7}$	$7.2\cdot10^{-7}$	$1.1\cdot10^{-6}$	$2.2\cdot10^{-10}$
$2.0\cdot10^{-12}$	$1.3\cdot10^{-11}$	$1.3\cdot10^{-12}$	$2.4\cdot10^{-12}$	$2.7\cdot10^{-17}$
$9.8\cdot10^{-14}$	$6.7\cdot10^{-13}$	$6.7\cdot10^{-14}$	$1.2\cdot10^{-13}$	$1.1\cdot10^{-18}$
$6.1\cdot10^{-13}$	$4.2\cdot10^{-12}$	$4.3\cdot10^{-13}$	$7.8\cdot10^{-13}$	$7.1\cdot10^{-18}$
$5.9\cdot10^{-14}$	$3.9\cdot10^{-13}$	$3.9\cdot10^{-14}$	$7.1\cdot10^{-14}$	$5.7\cdot10^{-19}$
$1.3\cdot10^{-11}$	$8.8\cdot10^{-11}$	$8.3\cdot10^{-12}$	$1.5\cdot10^{-11}$	$7.4\cdot10^{-17}$
$2.8\cdot10^{-15}$	$2.5\cdot10^{-14}$	$1.9\cdot10^{-15}$	$3.5\cdot10^{-15}$	$1.9\cdot10^{-20}$
$9.4\cdot10^{-16}$	$8.1\cdot10^{-15}$	$6.1\cdot10^{-16}$	$1.2\cdot10^{-15}$	$7.2\cdot10^{-21}$

17*

phenomenological form of the potential barrier for the $A_f + X$ pair was known, it was compared with the shape of the barrier for the folding potential. In all these cases the differences were not very large and were not taken into account, since the phenomenological optical potentials themselves were studied at fairly high (compared with the decay) energies, and the contribution of the exchange terms effectively included in these potentials depends on the energy.

In Table III we give the values of W_{Xc}^{cl} for various pairs X and A_f, calculated using the above potentials. The large variations of W_{Xc}^{cl} for a fixed channel c as a function of the choice of potential should be noted. For $X = {}^{14}$C they reach four orders of magnitude, for ^{24}Ne they reach seven, and for ^{28}Mg they reach eight. The results of the calculations can differ by three orders of magnitude for potentials 3 and 8, for which the differences between the barrier shapes are much smaller than the typical errors in extracting their parameters from the scattering data. We thus are faced with a serious problem which, in practice, did not arise in processes involving α particles, where the values of $W_{\alpha c}^{cl}$ for different folding potentials differ only by a factor of 5–6,[53] which is close to the uncertainties in calculating the absolute α-decay width.

Moreover, use of the data on the (n, α) reaction allows the size of these variations to be decreased by nearly a factor of two.

It should be noted that the spread in the variations of W_{Xc}^{cl} in the X-decay cases studied is roughly the same as when the purely Coulomb potential with a cutoff is used[10] for cluster–nucleus interactions if the cutoff radius is changed by about 15%. If we reject the principles for selecting potentials $V_{XA}^{nucl}(R)$ used above, the variations of W_{Xc}^{cl} increase by several orders of magnitude more. For example, the barrier for the proximity potential of Ref. 42 turns out to be higher than for all the potentials studied in Table III.

It is useful to compare the values of W_{Xc}^{cl} that we obtained with the experimental spectroscopic factors from Ref. 56 calculated using the same potential $V_{XA_f}^{nucl}$. As follows from Fig. 1 of Ref. 56 and Table III, numerically they are very close for all types of emitted clusters. However, the above discussion shows that the absolute values of the spectroscopic factors and to a certain degree their dependence on A_X contain serious ambiguities related to the choice of the nuclear potential for the cluster–nucleus interaction.

Fortunately, this conclusion is not valid for the relative

TABLE IV. Forbiddenness factors F_{Xc}^{exp} for various potentials.

A_i	$X+A_f$	1	2	3	4	5	6	7	8	$\overline{F}_{Xc}^{exp}$
^{223}Ra	^{14}C + ^{209}Pb	82	86	84	84	87	82	83	87	84
^{231}Pa	^{24}Ne + ^{207}Tl	13	14	14	13	13	13	13	15	13
^{233}U	^{24}Ne + ^{209}Pb	94	110	97	115	116	112	111	71	103

characteristics of cluster decay studied for a fixed particle X in narrow range of parent nuclei, in particular, for the even–odd effects discussed above. In fact, if in analogy with α decay we define the forbiddenness factor of a given decay into the channel c as

$$F_{Xc} = (W^{\text{cl}}_{Xc_0})_{\text{ev.ev}}/W^{\text{cl}}_{Xc}, \tag{23}$$

where $(W^{\text{cl}}_{Xc_0})_{\text{ev,ev}}$ is the spectroscopic factor of the decay into the same channel, averaged over the even–even parent nuclei adjacent to the nucleus in question, then, as shown in Table IV, the values of the factor F_{Xc} turn out to be practically independent of the choice of the potential V^{nucl}_{XA}. The F^{exp}_{Xc} thus determined also coincide up to a factor of 2–3 with the forbiddenness factors obtained from the simple systematics in Figs. 16 and 17.

The independence of F^{exp}_{Xc} from the choice of potential allows, first, the introduction of a quantitative measure of even–odd effects in cluster decay and, second, a classification of cluster decay without abandoning the nonadiabatic mechanism. By analogy with α decay, we shall refer to the cluster decay of an even–even parent nucleus A_i with emission of an even–even cluster as "favored," so that $J_i = J_f = 0$. Then a decay with emission of the same cluster from a neighboring $(A'_i = A_i \pm 1)$ odd nucleus with the condition that $J_i \neq J_f$ will be termed "semifavored." As will be discussed in more detail below, the values of the experimental forbiddenness factors F_{Xc} in the microscopic model of nonadiabatic cluster formation are quantitatively reproduced for emitted ^{14}C and ^{24}Ne nuclei when the shell structure of the cluster and of the parent and daughter nuclei is taken into account.

Microscopic schemes for calculating the spectroscopic factors of cluster decay

In order to demonstrate the theoretical competence of approaches to describing cluster decay based on analogs with α decay, it is necessary first to microscopically reproduce the phenomenological spectroscopic factors. Methods for calculating them theoretically for various types of cluster channels are described in detail in the monographs of Refs. 53 and 70. The complexity of the calculations of these quantities increases dramatically with increasing cluster mass, and the results are very sensitive to details of the structure of the cluster and of the parent and daughter nuclei.

Experience in calculating these quantities for the α decay of heavy nuclei, and also calculations for processes involving various clusters in light nuclei, shows that the most important problem is the inclusion of two factors: recoil of the residual nucleus toward the center of mass and configuration mixing owing to superfluid nucleon–nucleon correlations. Increase of the cluster mass leads to a sharp (practically exponential) enhancement of these effects. For understanding the results it is necessary to outline the main features of the formalism.

As usual,[70] we define the cluster form factor of the breakup of a nucleus A into a cluster X and a residual nucleus $(A - X)$ in the shell region as

$$\Phi_L(\rho) = \langle \hat{A}\{U^{J_i\pi_i M_i}_L \delta(\rho - \rho')\} \mid \psi^{J_i\pi_i M_i}\rangle, \tag{24}$$

where ρ is the relative coordinate of the centers of mass of the daughter nucleus and the cluster; $\psi^{J_i\pi_i M_i}$ is the translationally invariant internal shell function of the parent nucleus, characterized by angular momentum J_i, parity π_i, and angular-momentum projection M_i;

$$\hat{A} = \begin{pmatrix} A \\ X \end{pmatrix}^{1/2} \sum_P (-1)^p \hat{P} \tag{25}$$

is the antisymmetrization operator; $\hat{P}$ is an operator which permutes the nucleon coordinate labels of the fragments X and $(A - X)$; p is the parity of this permutation;

$$U^{J_i\pi_i M_i}_L = \{\psi^{J_f\pi_f}\psi^{J_X\pi_X} Y_L(\Omega_\rho)\}_{J_i\pi_i M_i} \tag{26}$$

is the channel function, characterized by the same quantum numbers as the parent-nucleus function; $\psi^{J_f\pi_f}$ and $\psi^{J_X\pi_X}$ are the translationally invariant shell functions of the daughter nucleus and the cluster, respectively; $Y_L(\Omega_\rho)$ is a spherical function.

The shell spectroscopic factor W^{sh}_X is expressed in terms of the cluster form factor in the shell region using the equation

$$W^{\text{sh}}_X = \int_0^\infty \Phi^2_L(\rho)\, \rho^2\, d\rho. \tag{27}$$

Following Ref. 70, it can be shown that for the smearing of the Fermi surface characteristic of a real nucleus,

$$\Phi_L(R_X) \simeq (-1)^L \left(\frac{A}{A-X}\right)^{n_{\min}/2} \Phi_{\text{sh}}(R_X), \tag{28}$$

where

$$\Phi_{\text{sh}}(R_X) = \langle \psi^{J_i\pi_i M_i}_{\text{sh}} \mid \hat{A}\{U^{J_i\pi_i M_i}_{\text{sh}L}\, \delta(R_X - R'_X)\}\rangle, \tag{29}$$

ψ_{sh} is the usual shell-model function,

$$U^{J_i\pi_i M_i}_{\text{sh}L} = \{\psi^{J_f\pi_f}_{\text{sh}}\psi^{J_X\pi_X} Y_L(\Omega_\rho)\}_{J_i\pi_i M_i}, \tag{30}$$

and $n_{\min}$ is determined by the minimum number of nodes $\nu_{\min}$ of the relative-motion function $\Phi_{\text{sh}}(R_\nu)$ allowed by the Pauli principle: $n_{\min} = 2\nu_{\min} + L$, which coincides with the analogous quantity in the oscillator model. In the end, in changing over to the functions ψ_{sh} in the equation for the cluster formation probability the factor $[A/(A-X)]^{n_{\min}}$ appears; its values are given in Table V, where we see that for emission of a ^{40}Ca nucleus this factor can reach 10^{12}.

Let us construct the formalism for computing the form factor (29). Since the function on the right-hand side is totally antisymmetric, it can be written as

$$\psi^{\text{sh}}(R_X) = \langle U^{J_i\pi_i M_i}_{\text{sh}}\, \delta(R_X - R'_X) \mid \psi^{J_i\pi_i M_i}_{\text{sh}}\rangle \begin{pmatrix} A \\ X \end{pmatrix}^{1/2} \tag{31}$$

TABLE V. Factors forming the recoil effect for various clusters.

X	N_X	$N = N_A - N_{A-A_X} - N_X$	$(A/(A-A_X))^N$
^{8}Be	4	40	4.5
^{12}C	8	58	25,9
^{14}C	10	68	83,9
^{16}O	12	76	279
^{20}Ne	20	90	$3,88\cdot10^{3}$
^{22}Ne	24	98	$1,9\cdot10^{4}$
^{24}Ne	28	106	$1,06\cdot10^{5}$
^{28}Mg	36	120	$3,82\cdot10^{6}$
^{34}Si	48	142	$2,17\cdot10^{9}$
^{40}Ca	60	160	$1,67\cdot10^{12}$

$A - A_X = A_f = 208$

All of the clusters X of interest to us fall into the category of light nuclei, and the oscillator model is fully justified for them.

To calculate the overlap integral (31) we write the wave function of the cluster internal motion $X\psi^{J_X\pi_X M_X}$ in the form of a multicluster representation, for brevity restricting ourselves to clusters X pertaining to the p shell. Then, selecting a partition of the group X into the required number of α particles, bineutrons, and, if necessary, a single neutron (proton), we obtain

$$|\psi^{J_X\pi_X M_X}\rangle \equiv |XN = X-4[f]L_XS_X\rangle$$
$$= a_{\{L_j\}}\hat{A}\{\prod_{i=1}^{\beta}(\psi_{\alpha_i})\prod_{k=1}^{\gamma}(\psi_{F_k})_{S_X}$$
$$\prod_{j=1}^{\beta+\gamma-1}[\varphi_{n_jl_j}(\rho_j)\{L_j\}L_X]\}_{J_X\pi_X M_X} \quad (32)$$

where $\{L_j\}$ is the set of intermediate angular momenta, which can be chosen arbitrarily with the only requirement that the selection rules be satisfied. For example, for $X = {}^{16}O$ it is convenient to take all the angular momenta $L_j = 0$, $l_j = 0$. In (32), ψ_{α_i} is the internal-motion function of a quadruplet of nucleons, and differs from the Gaussian wave function of an α particle only by the dimensional parameter $\hbar\omega = \hbar\omega_{^{16}O}$, and the coordinates of the nucleons in it are numbered $(4i-3)$–$4i$; ψ_{F_k} is the corresponding function for the light cluster of mass F_k [for an even–even nucleus with $N_X > Z_X$, this is a neutron pair, and for an odd nucleus it is a neutron pair or a neutron (proton) of spin S_X]; $\varphi_{n_jl_j}(\rho_j)$ are the wave functions of the Jacobi coordinates characterizing the system of β α particles and γ clusters F_k;

$$1/a_{\{L_j\}} = \langle XN = X-4[f]L_XS_X|\hat{A}|\prod_{i=1}^{\beta}(\psi_{\alpha_i})$$
$$\times\prod_{k=1}^{\gamma}(\psi_{F_k})\prod_{j=1}^{\beta+\gamma-1}[\varphi_{n_jl_j}(\rho_j)]L_X\rangle \quad (33)$$

is the normalization factor. If the function on the right-hand side of (32) is not to be identically zero, we require that $n_j = F_k$ $(\gamma > 1)$ if $\beta = 1$, and $n_1 = 4$, $n_j = F_k$ $(\gamma \geqslant 1)$ if $\beta = 2$, and so on. The equality (32) holds, since in the wave function on its right-hand side all the quantum numbers needed to classify the system, N, $[f]$, L_X, and S_X, are determined uniquely, and the wave function is antisymmetric and normalized. The normalization $1/a_{\{Lj\}}$ is the multicluster (in the case $\beta+\gamma=2$ it is the ordinary, two-fragment) spectroscopic factor for the breakup of the nucleus X into light clusters in the ground state. These quantities are defined and methods for calculating them are given in Ref. 71. We shall briefly describe how to calculate them below.

Let us return to expression (31). In this study we restrict ourselves to the case of an even–even cluster. We again make use of the antisymmetry of the right-hand side. Operation on it with the antisymmetrization operator from Eq. (9) leads to the result

$$\Phi_{\rm sh}(R_X) = \left[\frac{A!}{(A-X)!\,(4!)^{\beta}\prod_{k=1}^{\gamma}(F_k!)}\right]^{1/2}$$
$$\times a_0\Big\langle \psi_{\rm sh}^{J_f\pi_f M_f}\Big|\prod_{i=1}^{\beta}(\psi_{\alpha_i})\prod_{k=1}^{\gamma}(\psi_{F_k})\prod_{j=1}^{\beta+\gamma-1}[\varphi_{n_jl_j}(\rho_j)] : L_X = 0$$
$$\times Y_L(\Omega_{R_X})\,\psi_{\rm sh}^{J_f\pi_f}\,\delta(R_X - R'_X)\Big\rangle, \quad (34)$$

where the symbol a_0 implies that we are using the multicluster representation with $l_j = 0$, $L_j = 0$. In order to integrate over the variables of the nucleons of the daughter nucleus, it is obviously necessary to make a fractional-parentage expansion of the parent wave function. The form of the right-hand side of the overlap integral from (32), which is the product of the wave function of the residual nucleus and several light clusters, in which the sets of nucleon coordinate labels are fixed, indicates that the left-hand side can also conveniently be represented as the sum of products of nucleon groups of similar masses, i.e., it is convenient to use the multicluster fractional-parentage expansion rather than the usual two-fragment expansion.[72] By definition the multicluster fractional-parentage coefficient is the coefficient in the expansion of the totally antisymmetric function of the proton (neutron) subsystem of the nucleus A into the sum of products of functions of several antisymmetric proton (neutron) groupings. Here an individual product is not antisymmetric under the interchange of nucleons from one grouping to another. Then

$$|p_i\rangle = \sum_{\Delta,\,\varepsilon}\langle p_i\,|\,p_f(\Delta),\,p(\varepsilon)\rangle\,|\,p_f(\Delta)\rangle\,|\,p(\varepsilon)\rangle, \quad (35)$$

where $|p_i\rangle$ and $|p_f(\Delta)\rangle$ are the wave functions of the proton component of the parent and daughter nuclei, and Δ and ε are the sets of quantum numbers characterizing these functions.

The most convenient form of the function of the isolated nucleons is

$$|\,p(\varepsilon)\,\rangle = \prod_{r}^{Z_X/2}|\,p_r^{(2)}(\varepsilon_r)\,\rangle, \quad (36)$$

where $|p_r^{(2)}(\varepsilon_r)\rangle$ is the function of a two-proton pair. The coefficient of the transformation (35) is easily determined in terms of the usual binary fractional-parentage coefficients:

$$\langle p_i\,|\,p_f(\Delta)\prod_{r=1}^{Z_X/2}p_r^{(2)}(\varepsilon_r)\rangle$$
$$= \sum_{\{\Delta_r\}}\prod_{r=1}^{Z_X/2}\langle p_{f_{r-1}}(\Delta_{r-1})\,|\,p_{f_r}(\Delta_r)\,p_r^{(2)}(\varepsilon_r)\rangle, \quad (37)$$

where $|p_{f_r}(\Delta_r)\rangle$ is the wave function of the proton subsystem of the nucleus of charge $Z_A - 2r$, characterized by the set of quantum numbers Δ_r, with $|p_{f_0}\rangle \equiv |p_i\rangle$ and $|p_{fZ_X/2}(\Delta_{Z_X/2})\rangle \equiv |p_f(\Delta)\rangle$. Expression (37) includes a summation over the full set of quantum numbers $\{\Delta_r\}$ characterizing the intermediate states. Let us substitute expressions (35) and (37) into the form factor (34). We note that the variables characterizing the residual nucleus and the clusters α_i, F_k are separated from each other on both the left- and the right-hand sides of the overlap integral, and we integrate over them. Then

$$\Phi_{\rm sh}(R_X)=\left[\frac{A!}{(A-X)!\,(4!)^{\beta}\prod_{k=1}^{\gamma}(F_k!)}\right]^{1/2}$$

$$\times a_0\sum_{\{\Delta_r\}\{\varepsilon_r\}\{\Delta'_{r'}\}\{\varepsilon'_{r'}\}}\left\langle\prod_{i=1}^{\beta}\tilde{\Phi}^{\varepsilon_i\varepsilon'_i}_{\alpha_i}(R_{\alpha_i})\prod_{k=1}^{\gamma}\tilde{\Phi}^{\varepsilon'_{\beta+k}}_{F_k}(\mathbf{R}_{F_k})\right|$$

$$\times\left|\prod_{j=1}^{\beta+\gamma-1}[\varphi_{n_jl_j=0}(\boldsymbol{\rho}_j):L_X=0]\,Y_0(\Omega_{R_X})\,\delta(R_X-R'_X)\right\rangle, \tag{38}$$

where the primed indices denote the quantum numbers of the neutron subsystem,

$$\tilde{\Phi}^{\varepsilon_i\varepsilon'_i}_{\alpha_i}(\mathbf{R}_{\alpha_i})\equiv\langle p_i^{(2)}(\varepsilon_i)\,n_i^{(2)}(\varepsilon'_i)\mid\delta(R_{\alpha_i}-R'_{\alpha_i})\,\psi_{a_i}\rangle, \tag{39}$$

$$\tilde{\Phi}^{\varepsilon'_{\beta+k}}_{F_k}(\mathbf{R}_{F_k})\equiv\langle n^{(2)}_{\beta+k}(\varepsilon'_{\beta+k})\mid\delta(R_{2n_k}-R'_{2n_k})\,\psi_{F_k}\rangle \tag{40}$$

are the three-dimensional form factors of the α particles and clusters F_k for the configurations $\{\varepsilon_i,\varepsilon'_i\}$ and $\varepsilon_{\beta+k}$. The expression

$$\Phi^{\Delta_i\Delta_{i-1}}_{\alpha_i}(\mathbf{R}_{\alpha_i})=\left[\frac{[A-4(i-1)]!}{(A-4i)!\,4!}\right]^{1/2}$$

$$\times\sum_{\{\varepsilon_i\}\{\varepsilon'_i\}}\langle p_{f_{i-1}}(\Delta_{i-1})\mid p_{f_i}(\Delta_i)\,p_i^{(2)}(\varepsilon_i)\rangle\langle n_{f_{i-1}}(\Delta'_{i-1})\mid n_{f_i}(\Delta'_i)$$

$$\times n_i^{(2)}(\varepsilon'_i)\rangle\,\Phi^{\varepsilon_i\varepsilon'_i}_{\alpha_i}(\mathbf{R}_{\alpha_i}) \tag{41}$$

and the analogous expression for the bineutron are the usual three-dimensional form factors of the corresponding clusters in the ordinary shell model with configuration mixing. They differ, for example, from the form factor of the free α particle by the factor

$$\left[\frac{A-4(i-1)}{A-4i}\right]^{n_{\min}/2}\eta_\alpha,$$

arising because of the absence of the effect of recoil toward the center of mass and the difference between the parameters $\hbar\omega_X$ and $\hbar\omega_\alpha$ in the shell model. The quantity $\eta_\alpha^2=W_\alpha(\hbar\omega_X)/W_\alpha(\hbar\omega_\alpha)$ is easy to calculate theoretically. Altogether we arrive at the expression

$$\Phi_{\rm sh}(R_X)=a_0\sum_{\{\Delta_r\}\{\Delta'_r\}}\eta_\alpha^{\beta}\eta_{2n}^{\gamma}\prod_{i=1}^{\beta}(W_{\alpha_i}^{1/2})\prod_{k=\beta+1}^{\beta+\gamma}(W_{2n_k}^{1/2})$$

$$\times\left\langle\prod_{i=1}^{\beta}\Phi'^{\Delta_i\Delta_{i-1}\Delta'_i\Delta'_{i-1}}_{\alpha_i}(\mathbf{R}_{\alpha_i})\prod_{k=1}^{\beta}\Phi'^{\Delta'_k+\beta\Delta'_{k+\beta-1}}_{2n}(\mathbf{R}_{F_k})\right|$$

$$\times\left|\prod_{j=1}^{\beta+\gamma-1}[\varphi_{n_jl_j=0}(\boldsymbol{\rho}_j):L_X=0]\,Y_0(\Omega_\rho)\,\delta(R_X-R'_X)\right\rangle, \tag{42}$$

where

$$\Phi'^{\Delta}_i(\mathbf{R}_i)=\frac{1}{W^{1/2}}\Phi^{\Delta}(\mathbf{R}_i) \tag{43}$$

are the normalized three-dimensional form factors of the light clusters, and their normalizations

$$W_i\equiv\int\left|\Phi_i(R_i)\right|^2R_i^2dR_i \tag{44}$$

are by definition the spectroscopic factors.

We note that the scheme for calculating a_0 given by Eq. (33) and involved in expression (42) is based on techniques similar to those just used. The final expression is very compact:

$$1/a_0=[\prod_{j=1}^{\beta-1}(S_{\alpha_i})\prod_{k=1}^{\gamma}(S_{F_k})]^{1/2}, \tag{45}$$

where S_{α_i} and S_{F_k} are the spectroscopic factors of the corresponding light clusters arising in the successive emission of these clusters from the nuclei X, $X-F_k$, etc., with formation of intermediate nuclei in their ground states and having the parameter $\hbar\omega_i=\hbar\omega_X$. The values of a_0 for various clusters from the p and s–d shells are given in Table VI.

The procedure for calculating the form factor (42), which contains a large number of summation indices, can be simplified greatly by using the fact that this sum contains a dominant component. The point is that the spectroscopic factors W_α of transitions between O^+ ground states of nuclei with emission of an α particle or a bineutron are many times larger than the average values. This is a consequence of the coherent summation of the amplitudes in expression (41). Studies of α decay[53] show that the scale of this effect, which arises because of superfluid nucleon–nucleon correlations in the ground states of nonmagic nuclei, is approximately a 30-fold enhancement per nucleon pair. In the end, any term of the sum over Δ_r (Δ'_r) containing a state different from the O^+ ground state as one of the intermediate states is suppressed by a factor of $\sim10^3$. The collective paired vibrational excitations $J^\pi_{\rm coll}=2^+,4^+,\ldots$ are an exception. For them the amplitudes of α transitions $J^\pi_{\rm coll}\to O^+$ also significantly exceed the average ones, owing to coherent addition. However, here the sum of the amplitudes corresponding to the excitation of an intermediate level is small, so that these components cannot compete with the dominant one. Therefore, the approximation of neglecting the contribution of transitions for which there is no superfluid enhancement has practically no effect on the accuracy of the calculations. Here the spectroscopic factor for X decay has the form

$$W_X=\left(\frac{A}{A-X}\right)^{n_{\min}}\eta_{2n}^{2\gamma}a_0^2\,\eta_\alpha^{2\beta}\prod_{i=1}^{\beta}(W_{\alpha_i})\prod_{k=1}^{\gamma}(W_{F_k})\mathcal{J}_X,$$

$$\mathcal{J}_X=\int J_X^2(R_X)\,R_X^2\,dR_X, \tag{46}$$

where

$$J_X(R_X)=\langle\prod_{i=1}^{\beta}\Phi'^{\Delta_i\Delta_{i-1}\Delta'_i\Delta'_{i-1}}(\mathbf{R}_{\alpha_i})\prod_{k=1}^{\gamma}\Phi'^{\Delta'_k+\beta\Delta''_{k+\beta-1}}_{2n}(\mathbf{R}_{F_k})$$

$$\times\prod_{j=1}^{\beta+\gamma-1}[\varphi_{n_jl_j=0}(\boldsymbol{\rho}_j)\,L_X=0]\,Y_0(\Omega_{R_X})\,\delta(R_X-R'_X)\rangle \tag{47}$$

and is the quantity which is most difficult to calculate. However, the method developed in Ref. 53 for computing the analogous α-particle form factor from four one-nucleon functions by successive convolution of them with the internal functions of the α-particle Jacobi coordinates is fully applicable also to the calculation of $J_X(R_X)$, and in principle complications arise only because of the increase in the number of repeated integrations and the appearance of

TABLE VI. Change of the normalization coefficient of the wave function of the emitted cluster with increasing mass and charge.

X	a_0^2	a'^2_0	X	a_0^2	a'^2_0
^{8}Be	0.667	—	^{26}Ne	26.52	0.276
^{12}C	0.988	—	^{28}Mg	162.5	1.08
^{14}C	2.61	—	^{30}Mg	125.8	0.095
^{16}O	3.33	—	^{32}Si	235.9	0.082
^{20}Ne	14.6	—	^{34}Si	208.6	$9.68\cdot10^{-3}$
^{22}Ne	20.2	6.16	^{40}Ca	30.95	$4.56\cdot10^{-5}$
^{24}Ne	21.15	1.57			

weakly oscillating functions $\varphi_{n_j l_j}(\rho_j)$ in the integrals.

The overlap integrals $J_X(R_X)$ involved in the definition of the shell spectroscopic factor of the particle X were calculated using the following scheme. Since, as shown by theoretical calculations, the form of the α-particle (two-neutron) form factors $\Phi_\alpha(R_\alpha)$ $[\Phi_{2n}(R_{2n})]$ is practically unchanged for a wide range of nuclei with $A \gtrsim 208$ when pairing effects are included, all the factors $\Phi'_\alpha(R_\alpha)$ $[\Phi'_{2n}(R_{2n})]$, normalized to unity, were chosen to have, in the calculation of the form factor $\Phi_X(R_X)$ (29), a universal form coinciding with that of the form factors $\Phi'_\alpha(R_\alpha)$ $[\Phi_{2n}(R_{2n})]$ calculated for the ^{218}Rn nucleus. The wave functions for the relative motion of the α particles and neutron pairs involved in the definition of the internal wave functions Ψ_X of the particles X were chosen to have the oscillator form with dimensional parameter equal to $\hbar\omega_X$. The calculated values of the integrals $\mathcal{J}_X$ for various X by computer are shown in Table VII.

It is easy to extend this formalism to clusters X belonging to nuclei of the s–d shell. The only modification needed is related to the fact that the set of quantum numbers characterizing the function ψ, namely, N, $[f]$, L, and S, is insufficient, so that it is necessary to add to it the SU(3) index $(\lambda\mu)$ and write Eq. (32) in a representation of SU(3). Here the derivation of the equations carried out above for a p-shell cluster becomes very complicated, owing to the presence of a large number of Clebsch–Gordan coefficients of the group SU(3). The final expression for W_X coincides with (46) with the replacement $a_0 \to a'_0$, where

$$a'^2_0 = a_0^2 \langle (n_5)0\,(n_6)0\,0 \mid (\lambda_5\mu_5)\,0\rangle^2 \prod_{j_2=5}^{\beta+\gamma-1} \langle (\lambda_{j_2}\mu_{j_2})\,0\,(n_{j_2+2}0)0 \mid \times \mid (\lambda_{j_2+1}\mu_{j_2+1}\,0)\rangle, \qquad (48)$$

TABLE VII. Change of the overlap integral with increasing complexity of the emitted cluster.

X	$\mathcal{J}_X$	X	$\mathcal{J}_X$
^{8}Be	$1.09\cdot10^{-2}$	^{26}Ne	$1.5\cdot10^{-15}$
^{12}C	$0.92\cdot10^{-4}$	^{28}Mg	$2\cdot10^{-15}$
^{14}C	$0.77\cdot10^{-6}$	^{30}Mg	$2\cdot10^{-17}$
^{16}O	$0.67\cdot10^{-6}$	^{32}Si	$1.5\cdot10^{-17}$
^{20}Ne	$0.89\cdot10^{-8}$	^{34}Si	$1.5\cdot10^{-19}$
^{22}Ne	$0.34\cdot10^{-10}$	^{40}Ca	$4.1\cdot10^{-20}$
^{24}Ne	$0.24\cdot10^{-12}$		

and the overlap integral $\langle (\lambda_1\mu_1)l_1(\lambda_2\mu_2)l_2 \mid (\lambda\mu)l\rangle$ are the Clebsch–Gordan coefficients of the group SU(3). In addition to the approximations discussed above, the derivation of Eq. (48) contains another approximation: components associated with $l_j \neq 0$ or $L_j \neq 0$ are ignored. Direct calculation for $X = {}^{24}$Mg shows that their contribution to W_X is sufficiently small. The values of a'^2_0 are also given in Table VI. The appearance of the product of a rather large number of Clebsch–Gordan coefficients of the group SU(3) in the final expression for the spectroscopic factor W_X leads to the following: one of its factors which for light clusters tend to increase with increasing mass A_X begins to decrease, which should seriously affect the general behavior of the dependence of the spectroscopic factors $W_X(A_X)$. In addition, we note that the use of the j–j coupling scheme, which is more accurate than the SU(3) scheme for clusters of mass $A_X > 28$, leads to a decrease of the a'^2_0, but, since the overlap of the functions of these schemes $\langle \psi_X^{SU(3)} \mid \psi_X^{jj}\rangle$ is fairly large, the decrease is not very important and is neglected in the present study.

Equation (46) can be used to calculate the shell spectroscopic factors of particles X using the experimental α-particle shell spectroscopic factors as the W_α. These quantities W_α^{exp} can be calculated from the expression

$$W_\alpha = W_\alpha^{exp}\left(\frac{A}{A-4}\right)^{-N_\alpha}\eta_\alpha^2, \qquad (49)$$

related to the idea that the cluster and shell spectroscopic factors of α particles are similar. Using the facts that for all even–even nuclei with $A = 212$–240 we have the factor $[A/(A-4)]^{-N_\alpha} \approx 1.5$, and the experimental α-particle cluster spectroscopic factors W_α^{exp} lie in the range $10^{-2.4}$–$10^{-2.2}$, the experimental values of the factors W_α (49) turn out to be fairly close ($10^{-2.6}$–$10^{-2.4}$) η_α^2, so that to estimate them below we can take $W_\alpha \simeq 10^{-2.5}\,\eta_\alpha^2$. For W_{2n} we used the theoretical estimate $W_{2n}^{exp} = 10^{-0.2}$, which agrees well with the experimental value of W_α^{exp}. The values of η_α^2 are similar for all clusters $X \geqslant 12$, and for $\hbar\omega_\alpha = \hbar\omega_{^{16}O}$ they are $\eta_\alpha^2 \simeq 2.7$, while the η_{2n}^2 are close to unity.

It should be noted that in the decay of parent nuclei with $N \gtrsim 136$ in going to the region of daughter nuclei with $N \gtrsim 126$, as a rule, the equilibrium deformations β_{20} of the parent nuclei ($0.15 \leqslant \beta_{20} \leqslant 0.20$) differ significantly from those of the daughter nuclei ($\beta_{20} = 0$), which have a spherical shape. In principle, in an $Sp(2,R)$ model close to the simple shell model it is possible to calculate the forbiddenness factor γ_0^2 in the shell spectroscopic factor W_X related to

TABLE VIII. Change of the enhancement coefficient K_X of the cluster formation probability with increasing cluster complexity.

X	K_X	X	K_X
^{8}Be	$8\cdot10^{5}$	^{22}Ne	$2\cdot10^{16}$
^{12}C	$7\cdot10^{8}$	^{24}Ne	$5\cdot10^{17}$
^{14}C	10^{10}	^{28}Mg	$5\cdot10^{20}$
^{16}O	$7\cdot10^{11}$	^{34}Si	$1\cdot10^{25}$
^{20}Ne	$6\cdot10^{14}$	^{40}Ca	$3\cdot10^{29}$

the inclusion of the change of shape of the nucleus upon emitting the particle X.

For the above deformations the forbiddenness factor is close to 0.1. For example, in a transition of a parent nucleus with $\beta_{20}=0.20$ to a daughter nucleus ^{208}Pb ($\beta_{20}=0$) with emission of a fragment X, we have $\gamma_0^2=0.041$. However, when for W_α in (46) the experimental values of the shell α-particle spectroscopic factors $W_\alpha^{\exp}$ (49) are used, it is not necessary to include the factor γ_0^2, since it is automatically included in the $W_\alpha^{\exp}$.

The most important feature of the mechanism for heavy cluster radioactivity discussed in this study is the presence of a manifest superfluid-enhancement effect. It causes the dominant contribution to the spectroscopic factor to come from functions of neutron (proton) pairs with total angular momentum equal to zero. As was shown above, the enhancement coefficient is $k_X\simeq30$ per nucleon pair in going from the shell model which neglects correlations to the superfluid model in the expressions for the bineutron (biproton) spectroscopic factors. Here the enhancement coefficient of the α-particle spectroscopic factor is

$$k=\frac{W_{2p}^{sc}W_{2n}^{sc}}{W_{2p}^{sh}W_{2n}^{sh}}\simeq10^{3}$$

in nuclei with $A-X\sim208$. Since the effect of the superfluid properties of the nucleus on the other quantities in (46) can be neglected, the spectroscopic factor W_X in the transition $0^+\to0^+$ is enhanced by the W_α and W_{2n} factors appearing in it.

In spite of the fact that Eq. (46) is not suitable for quantitative calculations in the shell model, which neglects superfluid-type nucleon–nucleon correlations, for illustrative purposes we can obtain the enhancement coefficient K_X for the cluster X by introducing the values of the shell and superfluid spectroscopic factors of light clusters into (46). The results of this estimate are given in Table VIII, which demonstrates the extremely large scale of the effect. We note that the inclusion of superfluid correlations allows the almost complete elimination, for particles of mass $X\leqslant40$, of the structural prohibition[70] on the formation of a fairly heavy particle X in the ground state from the nucleons of one principal shell.

The calculated shell spectroscopic factors W_α^{sh} of heavy clusters of the p and s–d shells are given in Table IX together with the W_X^{cl} calculated using the potential of Ref. 65. In view of the uncertainties in the values of W_X^{cl} discussed above, the agreement between these quantities and W_X^{sh} is quite satisfactory. However, no real significance can be attached to this, since the choice of a different potential $V_{XA_f}^{nucl}$ increases W_X^{cl} and spoils the agreement. Meanwhile, the tendency for both quantities to vary with varying A and X turns out to be very similar, so that the results obtained using the potential from Ref. 65 can be used to predict the width of cluster radioactivity for a wide range of masses A and A_X.

Table IX shows the phenomenological scale of the spread in the values of W_X^{cl} for a fixed cluster emitted by various even–even nuclei: 10^1 for ^{24}Ne and 2.3×10^1 for ^{28}Mg, and also a reliable decrease of W_X^{cl} in odd nuclei. This is yet another consequence of the superfluid-pairing effect, which provides a natural explanation of the existence of transitions with various degrees of forbiddenness among nuclear decays with heavy-fragment emission. Zero-order transitions, which in the theory of α decay are termed favored, correspond to the pairing of all the neutrons and protons in the isolated nucleus. First-order forbidden transitions arise when the angular momenta of the parent and daughter nuclei are not equal to each other ($J_i\neq J_f$), which corresponds to the unpairing of one neutron or proton pair. Here the forbiddenness factor is $F\lesssim K_{2n}\simeq30$. Second-order transitions are associated with two unpaired pairs and are characterized by forbiddenness factors $F\lesssim(K_{2n})^2\simeq10^3$. This transition hierarchy can be extended to the case in which the order of forbiddenness is $A_X/2$.

Theoretical estimates of the suppression factors F_{Xc}^{th} for cluster decays with ^{14}C and ^{24}Ne emission in the case $J_i\neq J_f$ have been obtained in Ref. 73 in the diagonal approximation.

TABLE IX. Comparison of the shell W_X^{sh} and experimental W_X^{exp} spectroscopic factors.

X	W_X^{sh}	W_X^{exp} (parent nucleus)	X	W_X^{sh}	W_X^{exp} (parent nucleus)
^{8}Be	6.6(—7) *	—	^{28}Mg	1 5(—21)	2,0(—22) (^{234}U)
^{12}C	1.4(—9)	—			6,1(—22) (^{236}Pu)
^{14}C	5.9(—11)	2.0(—10) **			4,6(—21) (^{238}Pu)
^{16}O	3,2(—12)	—			
^{20}Ne	1,3(—14)	—			
^{22}Ne	1,1(—16)	—	^{30}Mg	5.7(—24)	—
^{24}Ne	7.0(—19)	7.1(—19) (^{232}U)	^{32}Si	5,1(—25)	2.1(—24) (^{238}Pu)
		7.8(—18) (^{234}U)	^{34}Si	5,0(—27)	—
			^{40}Ca	6,0(—33)	—
^{26}Ne	2,8(—21)	—			

*The symbol $(-n)$ denotes 10^{-n}.
**Averaged over ^{222}Ra, ^{224}Ra, and ^{226}Ra.

TABLE X. Comparison of the theoretical F_{XC}^{th} and experimental F_{XC}^{exp} forbiddenness factors for the cluster decay of odd parent nuclei.

Parent nucleus ($J_i^{\pi_i}$)	Daughter nucleus ($J_f^{\pi_f}$)	Emitted cluster	F_{XC}^{exp}	F_{XC}^{th}
^{223}Ra (1/2$^+$)	^{209}Pb (9/2$^+$)	^{14}C	84	360
^{231}Pa (3/2$^-$)	^{207}Tl (1/2$^+$)	^{24}Ne	13	50
^{233}U (5/2$^+$)	^{202}Pb (9/2$^+$)	^{24}Ne	103	160

Therefore, the values of F_{Xc}^{th} given in Table X can be viewed as upper limits on the forbiddenness factors. Thus, it can be stated that the theoretical approach discussed above satisfactorily reproduces even–odd effects in cluster decay without the introduction of fitted parameters. In ending our discussion of the results of calculations of the spectroscopic factors of cluster decay, it is relevent to note that such a scheme was first developed and realized in Refs. 74–76. It is interesting to observe that the structure of the quantities W_X^{sh} (46) differs from the phenomenological equation (17). In addition to products of the α-particle spectroscopic factors, (46) contains factors with a different behavior as the cluster mass increases. From this point of view it is difficult to give a microscopic justification of the simple and clear structure of the spectroscopic factor introduced in Ref. 56.

In Ref. 77 an attempt was made to calculate the cluster spectroscopic factors using the technique of Talmi–Moshinsky coefficients developed at the dawn of cluster physics. Calculated equations for $X = {}^{12}$C and ^{16}O are given. The awkwardness of the technique did not allow calculations to be made even for clusters from the p shell in the simple shell model of the parent nucleus.

An approach somewhat different from the formalism of Refs. 74 and 75 but based on the same premises has been developed in Ref. 78 for calculating the width of nuclear decays with ^{14}C cluster emission. The main difference in its theoretical scheme is the use of the "new" definition of the spectroscopic factor and the cluster form factor introduced in Refs. 79 and 80. The new shell form factor $\Phi_{Xc}^{\prime sh}(R)$ is obtained from the traditional one by using the expression

$$\Phi_{Xc}^{\prime sh}(R) = [1 - K(R, R')]^{-1/2}\,\Phi_{Xc}^{sh}(R), \qquad (50)$$

where $K(R, R')$ is the exchange nucleus of the integral equation of the resonating-group model.[81] From the theoretical point of view the new version takes into account nucleon exchange between the decay fragments in the exit channel more accurately. In the scheme of the pioneering studies of Ref. 82, the ratio of the new W_X^{new} and the traditional spectroscopic factors W_X^{new}/W_X turned out to be 3×10^2 for α decay (Ref. 80) and 4×10^8 for ^{14}C decay (Ref. 78). This naturally forced the authors of Ref. 80 to use wave functions of the parent and daughter nuclei which reduced configuration-mixing effects to a very small scale owing to superfluid pairing. Because of this, in the good quantitative description of favored α transitions difficulties arise with the description of semi- and unfavored α transitions. In some nuclei (^{209}Po, ^{211}Rn, ^{213}Ra) even in a model without configuration mixing the α-decay widths calculated in the new scheme are about 60 times higher than the experimental values. Several other problems arising in this scheme can also be mentioned.

The reason for this might be either the method[80] of seeking an equivalent interaction potential for the fragments in the exit channel with the required smooth matching to the shell and cluster form factors, or a significant effect on the calculations from the neglect of coupling to channels corresponding to excited fragment states. A return to the usual R-matrix scheme with the new form factor in Ref. 82 led to a sharp decrease in the ratio of the α-decay width in the new and old schemes: $\lambda_\alpha'/\lambda_\alpha$ is several times unity, i.e., in this case the difference between the schemes lies within their theoretical accuracy.

Meanwhile, the calculation of the widths of cluster-radioactivity processes in the new scheme is very important because large differences in the results can in principle make it possible to uniquely choose a particular scheme. The inter-fragment potential of Ref. 55 was used in Ref. 78. Configuration mixing was taken into account in the $1h_{9/2}$ and $2f_{7/2}$ shells for protons and in the $2g_{9/2}$, $3d_{5/2}$, and $1i_{11/2}$ shells for neutrons. Here the scale of the enhancement turned out to be $k^2 = 5$ for a single α particle. Recoil toward the center of mass was neglected. The uncertainties of the calculations are discussed in detail in Ref. 78. In some cases their estimate is overly optimistic. The methods of Ref. 78 allowed calculations only for emission of the ^{14}C nucleus. Here also an equation was proposed for parametrizing the spectroscopic factor $S(^{14}\text{C}) \sim [S(\alpha)]^{14/4}$, which was used in a slightly modified form in Ref. 56 (see above).

A scheme in which the cluster form factor is calculated using the solution of the inhomogeneous two-body Schrödinger equation with the shell form factor used as the source function was developed in Ref. 83 for application to cluster radioactivity. However, the methods used in Ref. 83 to calculate the shell form factors are questionable, and therefore the results of that study are not discussed in detail below.

The coupling of the channel containing unexcited fragments to other channels via a specially chosen interaction has been studied in Refs. 84 and 85. The perturbation theory used in the first study gives an enhancement of decay with ^{14}C emission by more than an order of magnitude owing to channel coupling. The exact solution of the system of equations in Ref. 85 showed that this factor is considerably smaller and close to unity in the present case. However, the results of Ref. 85 pertained to a range of energies higher than those characteristic of cluster radioactivity. In this sense the conclusions of Ref. 85 cannot be considered definitive. Nevertheless, we note that lowering the energy also lowers the coefficient for enhancement due to channel coupling.

TABLE XI. Comparison of the experimental and theoretical logarithms of the cluster decay periods $T_{1/2}$.

Type of decay	E_κ, MeV	Теоретические значения lg ($T_{1/2}$, с) по данным различных работ										Experimental values of log($T_{1/2}$, sec)
		[47]	[36]	[23]	[41]	[56]	[50]	[78]	[37]	[57]	Present study	
^{221}Fr (^{14}C)	29,28	14,4	16,0	15,2	16,0	15,5	—	—	—	14,6	16,2	$>15,8$
^{221}Ra (^{14}C)	30,34	14,3	—	14,1	14,8	14,2	12,6	—	—	13,8	15,0	$>14,4$
^{222}Ra (^{14}C)	30,97	11,2	13,4	11,2	11,6	11,8	11,2	13,1	13,5	12,2	11,8	11,0±0,06
^{223}Ra (^{14}C)	29,85	15,2	15,7	15,0	15,7	15,1	14,1	15,2	15,2	15,7	16,0	15,2±0,05
^{224}Ra (^{14}C)	28,63	15,9	18,2	16,0	16,8	16,2	15,0	16,9	17,4	16,6	16,6	15,9±0,12
^{225}Ac (^{14}C)	28,57	17,8	—	18,7	19,7	18,6	—	—	—	—	19,7	$>18,3$
^{226}Ra (^{14}C)	26,46	21,0	23,2	21,0	22,2	21,1	21,2	—	21,3	21,2	21,6	21,2±0,2
^{231}Pa (^{23}F)	46,68	25,9	—	26,0	25,5	—	—	—	23,5	—	—	$>25,4$
^{232}Th (^{24}Ne)	51,75	25,3	26,2	24,8	24,9	24,8	21,2	—	—	—	25,6	24,6±0,07
^{232}Th (^{26}Ne)	49,70	29,5	30,6	29,1	28,4	27,9	—	—	—	—	30,4	$>27,9$
^{231}Pa (^{24}Ne)	54,14	23,4	23,5	23,7	23,5	23,4	19,3	—	—	23,1	24,4	23,4±0,08
^{232}U (^{24}Ne)	55,86	20,8	22,0	20,7	20,0	20,8	16,5	—	—	20,5	21,1	21,0±0,1
^{233}U (^{24}Ne)	54,27	24,8	24,5	24,9	24,8	25,4	21,3	—	—	23,0	25,6	24,9±0,15
^{233}U (^{25}Ne)	54,32	25,0	24,7	25,1	24,4	—	—	—	22,9	—	—	
^{234}U (^{24}Ne)	52,81	26,1	27,0	25,8	25,7	25,6	—	—	—	—	26,0	25,3±0,05
^{234}U (^{26}Ne)	52,87	26,3	27,5	26,2	25,0	26,4	—	—	24,7	—	—	
^{234}U (^{28}Mg)	65,26	25,8	26,5	25,4	25,7	25,4	—	—	—	—	25,4	25,7±0,06
^{237}Np (^{30}Mg)	65,52	27,5	27,8	28,3	27,7	29,9	21,0	—	—	—	29,3	$>27,2$
^{236}Pu (^{28}Mg)	70,22	21,0	22,1	—	—	—	—	—	—	21,2	21,1	$\sim 21,7$
^{238}Pu (^{28}Mg)	67,32	25,7	26,5	25,9	24,6	25,8	—	—	—	—	26,0	25,7±0,25
^{238}Pu (^{30}Mg)	67,00	26,0	26,8	25,5	—	26,9	—	—	—	—	—	
^{238}Pu (^{32}Si)	78,95	25,1	26,4	25,7	—	25,7	—	—	—	—	25,9	25,3±0,16
^{241}Am (^{34}Si)	80,60	24,5	25,6	26,5	26,2	28,8	16,3	—	—	—	28,0	$>25,3$
$\sigma_{\lg T_{1/2}}$ *		0,45	1,4	0,26	0,7	0,35	3,0	1,3	1,5	0,9	0,7	

*rms deviation of the theoretical estimates from the experimental results.

5. DISCUSSION OF THE RESULTS AND PERSPECTIVES FOR EXPERIMENTAL AND THEORETICAL STUDIES OF CLUSTER RADIOACTIVITY

In Table XI we compile the results of the theoretical studies discussed above. The experimental half-decay periods and energies of the emitted clusters are also given to facilitate the comparison. The latter clearly indicate the cases for which experiment does not discriminate the type of cluster. From the pragmatic point of view the best description of the experimental data is given by Refs. 23, 29, 47, and 56, discussed in detail above and claiming to be alternative approaches. However, from the viewpoint of the physics of this decay it is interesting to note the quite satisfactory description of experiment, on the one hand, by Ref. 36, where the fission ideology was apparently followed most systematically, and, on the other, by Ref. 78 and also the work of the present authors (see also our earlier calculations in Refs. 74–76), in which the cluster formation factors were calculated microscopically by analogy with α decay and including the structure of the nuclei participating in the process.

At this stage of the investigations it is apparently impossible to draw any unambiguous conclusion about the cluster decay mechanism on the basis of this agreement.

It is true that the picture of nonadiabatic cluster formation in the decaying nucleus appears more promising and diversified. It gives a natural explanation of even–odd effects, and easily interprets the success of the simple cluster-decay period systematics and the absence of strong coupling between the yields of fragments from ordinary "statistical" fission and the yield of clusters with $E \simeq Q_X$. Let us consider the latter in more detail. The experimental yields of α particles, ^{14}C clusters from Ra nuclei, ^{24}Ne and ^{28}Mg clusters from ^{234}U nuclei, and also fission fragments are shown schematically on the same scale in Fig. 18. We see that if clusters and fission fragments are formed by jumping over a deformed barrier, the barriers for these two cases are quite different.

The results of Ref. 86, in which the reactions ^{233}U(n_{th},^{24}Ne) and ^{233}U(n_{th},f) on thermal neutrons were studied simultaneously, have recently been published. A yield of Ne nuclei with kinetic energy $E_{kin} \simeq Q_{^{24}Ne}$ was not observed at a level of 10^{-9} of binary fission, and a yield of Ne nuclei with $E_{kin} \sim Q_{Ne}/2$ owing to ternary fission has been observed. The experience gained in studying fission shows that the form of the mass distribution of fragments from spontaneous fission and from the reaction (n_{th},f) varies weakly. Therefore, extrapolation of the results of Ref. 86 to the case of spontaneous fission of the compound nucleus ^{234}U would lead one to expect a yield of cold ^{24}Ne and ^{210}Pb at a level certainly below 10^{-8} of fission, owing to the decrease of the ratio Q_X/B_X^{coul}. However, the experimental yields of fragments and of Ne nuclei are roughly equal (see Fig. 18). This indicates that it may not be correct to apply fission ideas directly to cluster decay. This conclusion is also consistent with our systematics of the experimental data on the cluster decay probability.

At the present time the experimental sensitivity in cluster detection allows detection of the effect down to $\lambda_{cl}/\lambda_\alpha \sim 10^{-16}$. The main thrust of the experimental studies has been and still is the study of the cluster radioactivity width Γ_X as a function of the mass number of the cluster X and, owing to the condition $A_i - A_X \simeq 208$, as a function of the mass number of the parent nucleus A_i. All the theoretical and phenomenological schemes and also the extrapolation of the experimental data predict that the ratio λ_X/λ_α falls off with increasing X, but the rate of falloff is different in different schemes. It is interesting to carry out experiments to observe cluster decay with ^{48}Ca emission. From the ex-

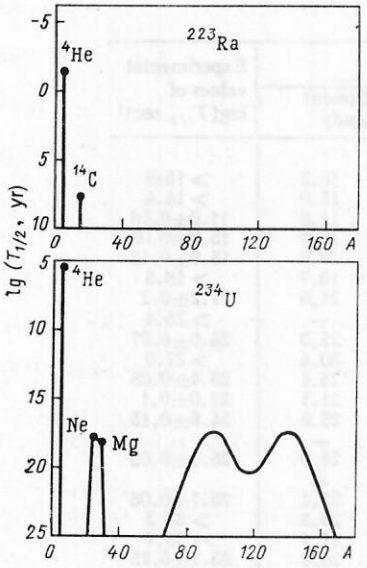

FIG. 18. Comparison of the probabilities for various types of radioactive decay (α decay, cluster emission, spontaneous fission) for ^{223}Ra and ^{234}U nuclei.

perimental point of view the most promising ^{48}Ca nucleus emitter is ^{249}Cf, which is available in quantities of the order of milligrams. Although most models predict small values of this ratio (for example, the theoretical estimates of the present authors give $\lambda_{Ca}/\lambda_\alpha \lesssim 10^{-30}$), even upper experimental limits can prove critical for eliminating some of the proposed models. Moreover, this is apparently where one should look for the transition to the fission regime.

The authors of Ref. 23 pointed out the possibility of using the ISOLDE-III setup at CERN to study ^{14}C emission from the odd–odd nucleus ^{220}Fr, ^{12}C emission from ^{114}Ba, and ^{8}Be emission from ^{186}Bi. Except for the first variant, working with such highly neutron-deficient nuclei in quantities of about 10^{10} nuclei appears to be very problematical.

Important information for analyzing the appearance of forbiddenness factors in cluster decay for an odd parent nucleus can be obtained by raising the sensitivity by two to three orders of magnitude in comparison with that attained in the experiments which have been carried out on the decay of ^{237}Np, ^{235}U, ^{233}U, and ^{231}Pa. In the case of ^{233}U it may be possible to observe decay with emission not only of ^{24}Ne, but also of ^{25}Ne separately. In the case of ^{231}Pa it is possible to observe decay with formation of ^{23}Fe in addition to the main branch ^{24}Ne. It is important to significantly increase the sensitivity in the study of decays of the even–even nuclei ^{232}Th, ^{236}U, and ^{240}Pu, for which so far only the limits of cluster decay have been determined. Our previous theoretical predictions for λ_X/λ_α are the following:

$^{235}\text{U} \rightarrow {}^{209}\text{Pb} + {}^{26}\text{Ne}$; $-\lg(\lambda_X/\lambda_\alpha) = 15.1$;
$^{235}\text{U} \rightarrow {}^{205}\text{Hg} + {}^{30}\text{Mg}$; $-\lg(\lambda_X/\lambda_\alpha) = 15.1$;
$^{236}\text{U} \rightarrow {}^{206}\text{Hg} + {}^{34}\text{Si}$; $-\lg(\lambda_X/\lambda_\alpha) = 14.3$;
$^{240}\text{Pu} \rightarrow {}^{206}\text{Hg} + {}^{34}\text{Si}$; $-\lg(\lambda_X/\lambda_\alpha) = 16.2$,

i.e., the observation of decay events is not hopeless.

Experimental searches for cluster decay to excited levels of the daughter nucleus are important for choosing the best theoretical models of cluster decay. Such experiments, which require an energy resolution of $\lesssim 1$ MeV, can apparently be carried out only using electronic techniques or magnetic spectrographs. Sources with high specific activity and small area must be used, which is possible only for relatively short-lived nuclei. It is possible that here again the optimal variant will be ^{223}Ra for decay with ^{14}C emission to the first excited levels in ^{209}Pb.

The change of the widths Γ_X of this transition relative to the widths of the transition between ground states is a consequence not only of the change of the barrier penetration factor, but also of the change of the forbiddenness factor F. Since the relative change of the penetration factor depends weakly on the choice of interaction potential, while the effect of changing the centrifugal barrier is negligible for cluster radioactivity, measurements of decays to excited states provide a direct determination of the forbiddenness factors. Moreover, they serve as a good test for choosing between models with widely different barrier thickness, i.e., adiabatic and nonadiabatic models. It would be very interesting to study the favored transition of an odd parent nucleus with emission of an even–even cluster to an odd daughter nucleus with angular momentum $J_f = J_i$. If here the forbiddenness factor, in contrast to transitions to other levels, proves to be small (several times unity), this will be convincing evidence in favor of a nonadiabatic mechanism of cluster formation, since for the "fission" mechanism even–odd effects can be related only to a change of the barrier—they are practically independent of the angular momentum J_f.

Theoretical predictions of the characteristics of transitions to various states of the ^{209}Pb nucleus in the decay $^{223}\text{Ra}(J^\pi = 1/2^+) \rightarrow {}^{14}\text{C}$ are given in Ref. 89. The calculations were carried out with assumptions analogous to those used in Ref. 73. The results indicate that the suppression factors depend strongly on the quantum characteristics of the states of the final nucleus.

The article of Ref. 90 appeared while we were writing this review. In that study the fine structure of ^{223}Ra decay was confirmed experimentally. The forbiddenness factor for transitions to the first two excited levels ($J_f^\pi = 11/2^+$ and $15/2^-$) turned out to be $\sim$2–5, while for the transition to the ground states it was more than 500. The first value of F_{Xc}^{exp} is characteristic of favored transitions, and the second is characteristic of semifavored and unfavored α transitions. In our opinion, the result of Ref. 90 is convincing proof of the analogy between the mechanisms for α decay and decays with emission of heavier clusters.

The decay mechanism changes in going to highly excited states of the parent nucleus.[74] Since the potential barrier for an α particle is much thicker than for clusters, the increase of the penetration factor in the latter case is much smaller.

Accordingly, the observation of heavy particles in such processes is problematical. This is confirmed by Ref. 88. A detailed discussion of these questions would take us far beyond our chosen topic.

The following topics are very important from the view-

point of developing the theory of cluster decay. It is necessary to take into account shell corrections in the calculation of the potential surfaces and the mass-parameter surfaces in the theory of adiabatic cluster formation. It is also important to solve the Schrödinger equation in a space of collective variables adequate for describing the evolution of the system along the trajectory corresponding to the minimum of the action integral.

In models of nonadiabatic cluster formation it is necessary to develop the theory of the forbiddenness factors for the case in which the parent and daughter nuclei differ significantly owing to deformation. It is equally important to determine the scale of the enhancement of the cluster decay probability owing to nucleon exchange in the exit channel,[84] taking into account the channel coupling due to the noncentral interaction. The effects of variations of the α-particle and cluster dimensions in the inclusion of superfluid correlations in *pp* and *nn* pairs in the parent nucleus also need to be refined.

An important theoretical argument in the determination of the cluster radioactivity mechanism might prove to be the development of a hybrid formalism which takes into account both adiabatic deformation and the formation factor (the shell spectroscopic factor) for a nucleus of this shape. This approach would make it possible to fix a certain state of the system in the exit channel and could perhaps describe both cluster decay and cold fission.

On the whole, the experimental discovery of cluster radioactivity has given new impetus to the development of theoretical ideas about nuclear rearrangement mechanisms in radioactive-decay processes.

The authors are grateful to Yu. Ts. Oganesyan and G. N. Flerov for their constant support and lively interest in this study, to V. P. Bugrov, Yu. S. Korotkin, I. A. Lebedev, B. F. Myasoedov, A. Sandulescu, G. A. Timofeev, D. Khashegan, and V. G. Chumin, who collaborated in the writing of many parts of this review, to the microscope and cyclotron laboratory workers at the JINR Laboratory of Nuclear Reactions, who played an important role in carrying out the experiments, and to the participants of a seminar at the JINR Laboratory of Neutron Physics for fruitful discussions of the theoretical part of this study.

[1]H. J. Rose and G. A. Jones, Nature **307**, 245 (1984).
[2]D. V. Aleksandrov, A. F. Belyatskiĭ, Yu. A. Glukhov *et al.*, Pis'ma Zh. Eksp. Teor. Fiz. **40**, 152 (1984) [JETP Lett. **40**, 909 (1984)].
[3]E. Rutherford, Philos. Mag. **27**, 488 (1914).
[4]D. N. Trifonov, *Radioactivity Yesterday, Today, and Tomorrow* [in Russian] (Atomizdat, Moscow, 1966).
[5]Yu. A. Shukolyukov, *Uranium Nucleus Fission in Nature* [in Russian] (Atomizdat, Moscow, 1970).
[6]A. Sandulescu, D. N. Poenaru, and V. Graĭner, Fiz. Elem. Chastits At. Yadra **11**, 1334 (1980) [Sov. J. Part. Nucl. **11**, 528 (1980)].
[7]B. G. Novatskiĭ and A. A. Ogloblin, Vestn. Akad. Nauk SSSR **1**, 81 (1988).
[8]S. Gales, E. Hourani, M. Hussonnois *et al.*, Phys. Rev. Lett. **53**, 759 (1984).
[9]W. Kutschera, I. Ahmad, S. G. Armato III *et al.*, Phys. Rev. C **32**, 2036 (1985).
[10]P. B. Price, J. D. Stevenson, S. W. Barwick *et al.*, Phys. Rev. Lett. **54**, 297 (1985).
[11]E. Hourani, M. Hussonnois, J. Stab *et al.*, Phys. Lett. **160B**, 375 (1985).
[12]A. Sandulescu, Yu. S. Zamyatnin, I. A. Lebedev *et al.*, JINR Rapid Communications No. 5-84, Dubna (1984), p. 5.
[13]S. W. Barwick, P. B. Price, and J. D. Stevenson, Phys. Rev. C **31**, 1984 (1985).
[14]A. Sandulescu, Yu. S. Zamyatnin, I. A. Lebedev *et al.*, Izv. Akad. Nauk SSSR, Ser. Fiz. **49**, 2104 (1985).
[15]S. P. Tret'yakova, A. Sandulescu, V. L. Mikheev *et al.*, Izv. Akad. Nauk SSSR, Ser. Fiz. **50**, 1925 (1986).
[16]S. P. Tret'yakova, A. Sandulescu, Yu. S. Zamyatnin *et al.*, JINR Rapid Communications No. 7-85 [in Russian], JINR, Dubna (1985), p. 23.
[17]P. B. Price and S. W. Barwick, in *Particle Emission from Nuclei, Vol. II*, edited by D. N. Poenaru and M. S. Ivuscu (CRC Press, Boca Raton, Florida, 1989), p. 205.
[18]D. V. Aleksandrov, Yu. A. Glukhov, E. Yu. Nikol'skiĭ *et al.*, Izv. Akad. Nauk SSSR, Ser. Fiz. **49**, 2111 (1985).
[19]A. Ya. Balysh, A. A. Gurov, and A. V. Demekhin, Zh. Eksp. Teor. Fiz. **91**, 37 (1986) [Sov. Phys. JETP **64**, 21 (1986)].
[20]Yu. S. Zamyatnin, Communication R6-86-821 [in Russian], JINR, Dubna (1986).
[21]S. Wang, P. B. Price, S. W. Barwick *et al.*, Phys. Rev. C **36**, 2717 (1987).
[22]S. P. Tretyakova, Yu. S. Zamyatnin, V. N. Kovantsev *et al.*, Preprint E7-88-803, JINR, Dubna (1988).
[23]P. B. Price, in *Proceedings of the International Conference on Fifty Years of Research in Nuclear Fission* (West Berlin, April 3–7, 1989); Nucl. Phys. (in press, 1989).
[24]P. B. Price, in *Proceedings of the Fifth International Conference on Nuclei Far from Stability* (Rossean Lake, Ontario, Canada, 1987), edited by I. S. Towner (American Institute of Physics, New York, 1988), p. 800.
[25]S. W. Barwick, Ph.D thesis, University of California, Berkeley (1986).
[26]S. P. Tretyakova, A. Sandulescu, and V. L. Mikheev, JINR Rapid Communications No. 13-85, JINR, Dubna (1985), p. 34.
[27]G. N. Flerov, D. S. Klochkov, V. S. Skobkin, and V. V. Terent'ev, Dokl. Akad. Nauk SSSR **118**, 69 (1958) [Sov. Phys. Dokl. **3**, 59 (1958)].
[28]A. A. Ogloblin, S. P. Tret'yakova, N. I. Venikov *et al.*, JINR Rapid Communications No. 2(35)-89 [in Russian], JINR, Dubna (1989), p. 43.
[29]D. N. Poenaru, W. Greiner, K. Depta *et al.*, At. Data Nucl. Data Tables **34**, 423 (1986).
[30]M. Paul, I. Ahmad, and W. Kutschera, Phys. Rev. C **34**, 1980 (1986).
[31]K. Y. Moody, E. K. Hulet, S. Wand *et al.*, Phys. Rev. C **36**, 2710 (1987).
[32]S. W. Barwick, H. L. Ravn, and P. B. Price, Phys. Rev. C **34**, 362 (1986).
[33]R. L. Fleischer, P. B. Price, and R. M. Walker, *Nuclear Tracks in Solids: Principles and Applications* (University of California Press, Berkeley, 1975) [Russian transl., Énergoizdat, Moscow, 1981].
[34]S. P. Tretyakova, P. Apel, L. Jolos *et al.*, in *Proceedings of the Tenth International Conference on Solid State Nuclear Track Detectors*, edited by H. Francois *et al.*) (Pergamon, Oxford, 1980), p. 283.
[35]Yu. P. Gangrskiĭ, Dalkhsuren and B. N. Markov, *Nuclear Fission Fragments* [in Russian] (Énergoatomizdat, Moscow, 1986).
[36]G. A. Pik-Pichak, Yad. Fiz. **44**, 1421 (1986) [Sov. J. Nucl. Phys. **44**, 923 (1986)].
[37]V. A. Rubchenya, V. P. Éĭsmont, and S. G. Yavshits, Izv. Akad. Nauk SSSR, Ser. Fiz. **50**, 1016 (1986).
[38]V. A. Rubchenya and S. G. Yavshits, Yad. Fiz. **40**, 649 (1984) [Sov. J. Nucl. Phys. **40**, 416 (1984)].
[39]V. M. Strutinsky, Nucl. Phys. **A122**, 1 (1968).
[40]Shi Yi-Jin and W. J. Swiatecki, Phys. Rev. Lett. **54**, 300 (1985).
[41]Shi Yi-Jin and W. J. Swiatecki, Nucl. Phys. **A438**, 450 (1985); **A464**, 205 (1987).
[42]J. Blocki, J. Randrup, W. J. Swiatecki *et al.*, Ann. Phys. (N.Y.) **105**, 427 (1977).
[43]D. N. Poenaru and M. Ivascu, Report NP-39, Central Institute of Physics, Bucharest (1984).
[44]D. N. Poenaru, M. Ivascu, A. Sandulescu, and W. Greiner, J. Phys. G **10**, L183 (1984).
[45]D. N. Poenaru, M. Ivascu, A. Sandulescu *et al.*, Phys. Rev. C **32**, 572 (1985).
[46]I. Perlman and J. O. Rasmussen, "Alpha radioactivity," in *Handbuch der Physik*, edited by S. von Flügge (Springer-Verlag, Berlin, 1957), Vol. 42, p. 109.
[47]D. N. Poenaru, M. Ivascu, D. Mazilu *et al.*, Report NP-54-86, Central Institute of Physics, Bucharest (1984).
[48]W. Greiner, M. Ivascu, D. N. Poenaru *et al.*, in *Treatise on Heavy Ion Science*, edited by D. A. Bromley (Plenum, New York, 1989), p. 343.
[49]R. K. Gupta, S. Gilaty, S. S. Malik *et al.*, J. Phys. G **13**, L27 (1987).
[50]F. Kumar, R. K. Puli, S. Singh *et al.*, in *Proceedings of the International Conference on Fifty Years of Research in Nuclear Fission* (West Berlin, 1989), p. 9.
[51]Pan Zhengying, Yuan Zhushu, and Yang Fuchia, Chin. Phys. Lett. **3**, 145 (1986); G. Shanmugam and B. Kamulaharan, Phys. Rev. C **38**, 1377 (1988).

[52]H. A. Bethe, *Elementary Nuclear Theory* (Wiley, New York, 1947) [Russ. transl., OGIZ, Moscow, 1948].
[53]S. G. Kadmenskiĭ and V. I. Furman, *Alpha Decay and Related Nuclear Reactions* [in Russian] (Énergoatomizdat, Moscow, 1985).
[54]M. Iriondo, D. Jerrestam, and R. G. Liotta, Nucl. Phys. **A454**, 252 (1986).
[55]P. R. Christensen and A. Winter, Phys. Lett. **65B**, 19 (1976).
[56]R. Blendowske and H. Walliser, Phys. Rev. Lett. **61**, 1930 (1988).
[57]A. F. Grashin and A. D. Efimenko, Yad. Fiz. **43**, 1330 (1986) [Sov. J. Nucl. Phys. **43**, 854 (1986)].
[58]S. G. Kadmenskiĭ, S. D. Kurgalin, V. I. Furman, and Yu. M. Chuvil'skiĭ, Preprint R4-89-509 [in Russian], JINR, Dubna (1989).
[59]D. A. Goldberg and S. M. Smith, Phys. Rev. Lett. **29**, 500 (1972).
[60]D. A. Goldberg, Phys. Lett. **55B**, 59 (1975).
[61]S. Saito, Prog. Theor. Phys. **41**, 705 (1969).
[62]O. M. Knyaz'kov, Fiz. Elem. Chastits At. Yadra **17**, 318 (1986) [Sov. J. Part. Nucl. **17**, 137 (1986)].
[63]C. M. Perey and R. J. Perey, At. Data Nucl. Data Tables **17**, 1 (1976).
[64]R. C. Barrett and D. F. Jackson, *Nuclear Sizes and Structure* (Clarendon Press, Oxford, 1977) [Russ. transl., Naukova Dumka, Kiev, 1981].
[65]F. P. Gareev, S. P. Ivanova, and B. N. Kalinkin, Izv. Akad. Nauk SSSR, Ser. Fiz. **32**, 1690 (1968).
[66]F. Becchetti and G. W. Greenless, Phys. Rev. **182**, 1190 (1969).
[67]G. R. Satchler and W. G. Love, Phys. Rep. **55**, 183 (1979); L. D. Rickertsen and G. R. Satchler, Phys. Lett. **66B**, 9 (1977).
[68]O. M. Knyaz'kov and E. F. Hefter, Z. Phys. A **301**, 277 (1981).
[69]G. R. Satchler, Nucl. Phys. **A329**, 233 (1979).
[70]O. F. Nemets, V. G. Neudachin, A. T. Rudchik *et al.*, *Nucleon Associations in Nuclei and Multinucleon Transfer Reactions* [in Russian] (Naukova Dumka, Kiev, 1988).
[71]L. Ya. Glozman and Yu. M. Chuvil'skiĭ, in *Problems in Nuclear and Cosmic Ray Physics* [in Russian] (Khar'kov State University Press, Khar'kov, 1986), Vol. 26, p. 43.
[72]L. Ya. Glozman and Yu. M. Tchuvil'sky, J. Phys. G **9**, 1033 (1983).
[73]V. P. Bugrov, S. G. Kadmenskiĭ, V. I. Furman, and Yu. M. Chuvil'skiĭ, *Nuclear Spectroscopy and Nuclear Structure* [in Russian] (Nauka, Leningrad, 1988), p. 474.
[74]S. G. Kadmenskiĭ, V. I. Furman, and Yu. M. Chuvil'skiĭ, Communication R4-85-368 [in Russian], JINR, Dubna (1985).
[75]S. G. Kadmenskiĭ, V. I. Furman, and Yu. M. Chuvil'skiĭ, in *Proceedings of the International School on Nuclear Structure, Alushta, 1985*, D4-85-851 [in Russian] (JINR, Dubna, 1985), p. 985.
[76]S. G. Kadmenskiĭ, V. I. Furman, and Yu. M. Chuvil'skiĭ, Izv. Akad. Nauk SSSR, Ser. Fiz. **50**, 1786 (1986).
[77]A. Florescu, S. Holan, and A. Sandulescu, Rev. Roum. Phys. **33**, 131 (1988).
[78]R. Blendowske, T. Fliessbach, and H. Walliser, Nucl. Phys. **A464**, 75 (1987).
[79]H. Feschbach, A. K. Herman, and R. N. Lemmer, Ann. Phys. (N.Y.) **41**, 230 (1967).
[80]T. Fliessbach and H. J. Wang, Nucl. Phys. **A263**, 75 (1976).
[81]K. Wildermuth and Y. C. Tang, *A Unified Theory of the Nucleus* (Academic, New York, 1977) [Russ. transl., Mir, Moscow, 1980].
[82]I. Tonozuka and A. Arima, Nucl. Phys. **A323**, 45 (1979).
[83]M. Ivascu and I. Silisteanu, Nucl. Phys. **A485**, 93 (1988).
[84]S. Landowne and C. H. Dasso, Phys. Rev. C **33**, 387 (1986).
[85]A. V. Tarakanov and V. M. Shilov, Communication R7-87-482 [in Russian], JINR, Dubna (1987).
[86]B. Börfig, P. Geltenbort, F. Gönnenwein *et al.*, in *Proceedings of the International Conference on Fifty Years of Research in Nuclear Fission* (West Berlin, 1989), p. 10.
[87]Yu. A. Lazarev, Yu. Ts. Oganessian, I. V. Shirokovski *et al.*, Europhys. Lett. **4**, 893 (1987).
[88]Yu. P. Gangrskiĭ, Kh. G. Khristov, and V. M. Bas'ko, Yad. Fiz. **44**, 294 (1986) [Sov. J. Nucl. Phys. **44**, 184 (1986)].
[89]V. P. Bugrov, S. G. Kadmenskiĭ, V. I. Furman, and Yu. M. Chuvil'skiĭ, in *Nuclear Spectroscopy and Nuclear Structure* [in Russian] (Nauka, Leningrad, 1987), p. 439.
[90]L. Brillard, A. G. Elani, and E. Hourani, in *Proceedings of the International School–Seminar on Heavy Ion Physics* (JINR, Dubna, 1989), p. 112.

Translated by Patricia Millard